PARAMETER-INDUCED SIMULATION OF CLIMATE CRASHES USING NEURO-FUZZY MODEL

A THESIS SUBMITTED TO THE GRADUATE SCHOOL OF APPLIED SCIENCES OF NEAR EAST UNIVERSITY

By
MOHAMMED AZAD OMAR

In Partial Fulfilment of the Requirements for The Degree of Master of Science in Computer Engineering

NICOSIA, 2018

PARAMETER-INDUCED SIMULATION OF CLIMATE CRASHES USING NEURO-FUZZY MODEL

A THESIS SUBMITTED TO THE GRADUATE SCHOOL OF APPLIED SCIENCES OF NEAR EAST UNIVERSITY

By
MOHAMMED AZAD OMAR

In Partial Fulfilment of the Requirements for The Degree of Master of Science in Computer Engineering

NICOSIA, 2018

Muhammad Azad Omer: PARAMETER-INDUCED SIMULATION OF CLIMATE CRASHES USING NEURO-FUZZY MODEL

**Approval of Director of Graduate School of
Applied Sciences**

Prof. Dr. Nadire ÇAVUŞ

We certify this thesis is satisfactory for the award of the degree of Master of Science in Computer Engineering

Examining Committee in Charge:

Assist. Prof. Dr. Boran ŞEKEROĞLU   Department of Information System
                                                  Engineering, NEU

Assist. Prof. Dr. Elbrus Bashir IMANOV   Department of computer engineering
                                                  Engineering, NEU

Prof. Dr. Rahib H. ABIYEV   Supervisor, Department of computer
                                                  Engineering, NEU

I hereby declare that all information in this document has been obtained and presented in accordance with academic rules and ethical conduct. I also declare that, as required by these rules and conduct, I have fully cited and referenced all material and results that are not original to this work.

Name, Last name:

Signature:

Date:

To my parents..…

ACKNOWLEGMENTS

ABSTRACT

The study focuses on determining whether there are any crashes or failure that are associated with the use of climate models when its parameters are induced to simulation. The study also focuses on analysing conditions that can cause climate models to fail because climate models are prone to failure, it become an important to determine chances of failure of the moodels. For this purpose in this thesis the neuro-fuzzy models is designed to determine chances of failure of the models. Consequently the aim was to develop solutions can be used to enhance the success or usefulness of models. The study used Takagi-Sugeno-Kang (TSK) type fuzzy rules for conducting neuro-fuzzy model which was used in simulation of climate crashes. For comparative analysis Support Vector Machines (SVM) is applied for simulation of the same problem. SVM is modelled using LibSVM package. A comparison was made between SVM and neuro-fuzzy model results to determine which algorithm offers the best simulation results. Accuracy rates of 94.4% and 95.55% were obtained for SVM and neuro-fuzzy model of the simulations. However, the neuro-fuzzy model was discovered to be having better performance in modelling climate crashes. Observations were also made that the POP2 of the CCSM4 was characterised with simulation failures. Research findings revealed that numerical reasons accounted for 8.5% of the simulation failures.

Keywords: Community Climate System Model; Failure Analysis; Neuro-Fuzzy model; Parallel Ocean Program; Simulation

ÖZET

Çalışma yerleri, parametreleri simülasyona yönlendirildiğinde iklim modellerinin kullanımı ile ilgili herhangi bir çökme veya arıza olup olmadığının belirlenmesine odaklanmaktadır. Çalışma aynı zamanda iklim modellerinin başarısız olmasına neden olan koşulların analizine odaklandı. Bu, iklim modellerinin her zaman başarısızlık eğiliminde olduğu düşünceleri, modellerin başarısızlık ihtimalini belirlemek için de nöro bulanık model de kullanıyor. Sonuç olarak, bu, modellerin başarısını veya yararlılığını arttırmak için kullanılabilecek çözümler geliştirmeyi amaçlıyordu. Çalışma, iklim çökmelerinin simülasyonunda kullanılan nüro-bulanık modeli yürütmek için Takagi-Sugeno-Kang (TSK) tipi bulanık kuralları kullanmıştır. Karşılaştırmalı analiz için aynı problemin simülasyonu için Support Vector Machines (SVM) uygulanmaktadır. SVM, LibSVM paketi kullanılarak modellenmiştir. Hangi algoritmanın en iyi simülasyon sonuçlarını sunduğunu belirlemek için SVM ve nöron bulanık model sonuçları arasında bir karşılaştırma yapılmıştır. Simülasyonların SVM ve nöronal bulanık modelleri için doğruluk oranları sırasıyla 94.4% ve 95.55% bulunmuştur. Bununla birlikte, nöron bulanık modelin iklim çökmelerinin modellenmesinde daha iyi performansa sahip olduğu keşfedildi. CCSM4'ün POP2'sinin simülasyon hataları ile karakterize edildiği gözlemleri yapıldı. Araştırma bulguları, sayısal nedenlerin simülasyon başarısızlıklarının 8,5% 'ini oluşturduğunu ortaya koymuştur.

Anahtar Kelimeler: Topluluk İklimsel Sistem Modeli; Hata Analizi; Nöro-Bulanık Model; Paralel Okyanus Programı; Simülasyon

TABLE OF CONTENTS

LIST OF FIGURES

LIST OF TABLES

LIST OF ABBREVIATIONS

CCSM4:   Community Climate System Model Version 4

CFL: Courant–Friedrichs–Lewy

CM: Climate Model

GCMS: Global climate models

POP: Parallel Ocean Program

RMSE: Root Mean Square Errors

SVM: Support Vector Machines

UQ: Uncertainty Quantification

TSK: Takagi-Sugeno-Kang

NFM: Neuro-Fuzzy Model

CHAPTER 1
INTRODUCTION

1.1 State of Problem of Climate model Crashes

Though climate models are considered to be offer huge benefits, they are still attracting a lot of criticisms and such criticism is tied to the idea that they suffer from failure which is known as crashes or bifurcations. Other researchers have gone to a large extent of attributing such failures to complexities that are as a result of their nature (Eastbrook, 2010; Rugaber et al., 2011; Sternsrud, 2009).

One of the notable issues surrounding the use of climate models is software challenges. That is, scientific representation problems tend to be high when the models involved are considered to be too complex (Farrell et al., 2011). However, the National Research Council (2012), established that modern tools such as uncertainty quantification (UQ), can be utilized to identify simulation model problems. Such is important because the obtained findings can be utilized to further improve model development. In climate modelling, primary UQ will be consisting of parameters or coefficients whose values are changeable. However, Sternsrud (2009), considers that this normally leads to simulating difficulties especially which makes it difficult to undertake at the desired resolutions. In most cases, parameterization will be done separately so that their responses are independent of each other and the best apparatus of achieving this is using non-linear climate models that are linked to other different parameterizations. Huge changes in simulation output are attained when the adjustable parameters are amplified using small perturbations but chances are high that the simulation is bound to fail (Gent et al., 2011).

In this study, findings are based on crashes that have been observed during simulation involving perturbed parameter UQ ensembles of the Community Climate System Model Version 4 (CCSM4). An assumption was made that binary outcome flag and input parameter values are known and this helped to determine if the simulation was complete or had failed.

Despite the availability of studies that have used UQ strategies in sought to determine whether different crashes can be noticed, the results have to a large extent been similar (Gent et al., 2011; Jackson et al., 2008; Webster et al. 2004). However, the frequency at which they occur is

established to be high and there exist other cases which have not been documented. Sanderson (2011) also contends that there is also an element of reporting bias.

1.2 Literature Review

Randall et al. (2007) conducted an evaluation of climate models and their ability to predict future climate changes. The credibility of climate models varies between parameters. For instance, the findings showed that climate variables such as precipitation tend to have lower predictability power as compared to their ability to forecast temperature changes. The results, however established that numerous improvements have been made to enhance the use and effectiveness of climate models. Such improvements include interactive aerosols and can now simulate essential elements such as Madden-Julian Oscillation and the El Nino-Southern Oscillation.

Jones et al. (2009) have considered the use of climate data to forecast future climate changes using a General Circulation Model. The study uses stochastic and generalized downscaling methods to generate the data so as to be capable of providing weekly data. Just like global climate models, the results revealed that uncertainties tends to affect the extent to which downscaling can be used to generate climate model data. The study also recommends that using various simulation models and scenarios is important so as to enable potential climate changes and their implications.

Van Vuuren et al. (2011) conducted a study to examine the extent to which integrated climate models simulate climate changes. The study placed focus on integrated assessment models to evaluate environmental policies targeted at reducing emissions and combines uncertainty quantification methods to simulate carbon components. The findings showed that most simulated findings established by climate models do fall within the expected range of forecasts especially those of complex models. Thus improvements in climate models extends to cover carbon cycle feedbacks, inertia and climate sensitivity.

Beaumont et al. (2008) undertook a study to examine how the choice of future climate scenarios for species distribution modelling important. The study established that modelling uncertainties are as a result of using different climate models. As a result, the study used species distribution models and the findings showed that careful selection of climate models is an important process which must not be done arbitrary. The findings also provide recommendations climate scenarios

must be those that relate to the situation under study and if not then uncertainty in assessments might trigger different climate change results.

Koutsoyiannis et al. (2008) did a study to analyze the credibility of climate predictions. Arguments were levelled on the idea that climate models are relatively used by little has been done to examine their reliability. Comparisons were made between model outputs collected from eight stations and the results showed that local models are not usually correct and that the idea that models have a tendency to perform better at a high scale.

Lamarque et al. (2013) conducted a climate diagnostics, simulation and description of climate models drawing examples from the Atmospheric Chemistry and Climate Model Intercomparison Project. Modern day climate forecasts (zonal wind, humidity, temperature and precipitation were established to be having bias levels that are similar to modern day climate modelling apparatuses. Consistent model results were established to exist between zonal winds of 2000 to 21000 and from 1850 to 2000.

Jones and Thornton (2013) used data generation and generalized downscaling using general circulation model using a combination of weather generalization, climate typing and empirical downscaling. A MarkSimGCM software was used and the results showed that certain climate models must be manipulated before they can be used to forecast climate changes.

Haggemann et al. (2013) did an assessment of how climate change influences water resources using hydrology and several global climate models. The idea is based on the fact that climate change triggers the changes that affect the availability of water and thus uses eight hydrological models and three global climate models to assess such effects. The findings showed that climate changes in the hydrology were causing changes in water reservoirs and hence conclusions were made that climate models are responsible for major uncertainties that are observed with climate models. Modellings errors were observed to be as a result of the choice made over models and such errors are considered to be smaller for climate models than those caused by hydrology models.

Several ideas have been given surrounding the use of climate models and such ideas tend to differ on complexity and success perspectives. For instance, Gent et al. (2011), posits that prevailing climate models are characterized with complexities which are in most cases considered to be extraordinary. This was supported by ideas given by Randall et al. (2007), who established that

climate models consists of various subroutines, functions, algorithms (geologic, climate and biological), tons of lines of codes. All these are utilized to deal with conservative laws and equations of state for momentum, energy and flow of matter within the earth's reservoirs, between the land, oceans and atmosphere. All these ideas are based on views that climate models are not always reliable and effective, and are bound to fail (Easterbrook & Johns, 2009; Washington & Parkinson, 2005). There are no concrete reasons and concurrences about what triggers a failure in climate models. For instance, Easterbrook and Johns (2009), strongly believe that the use of numerous algorithms of anthropogenic, geologic, chemical and biological nature that are used in the simulation of climate related issues and greenhouse gases, ozone, aerosols, Sulphur, nitrogen, and cycles of carbon is the main cause of climate model failure. This problem is made worse by the idea such algorithms are utilized in a lot of circumstances and time, and have solid, liquid and gaseous elements (Edwards et al., 2011). Alternatively, Clune and Rood (2011), revealed that software design and implementation problems can also necessitate vulnerability of climate models. This is because they are developed through a process that involves agile and huge open source software projects. Furthermore, other studies contend that the list of documented cases of crashes is high but little has been done to document important crash observations. This follows observations that have been made by Webster et al. (2011), that crashes tend to occur at a high rate but the number of recorded cases is very low. Hence, this further implies that a new study is required to further add and refurbish existing information about crashes in climate models. Irrespective of such an observation, ideas are still different and contrasting to each other and common consensus about the causes of crashes is still low and not continues to differ by study. For instance, bifurcations or crashes are common in any situation irrespective of its complexity and went to establish that intermediate climate models are also prone to crashes. To make matters worse different reasons behind such bifurcations are still different. For instance, Stainforth et al. (2005), attributes the causes to positive model feedbacks while Shiogama et al. (2012), attributes such causes to numerical instabilities such as collapse of the Atlantic meridional overturning circulation. This study therefore seeks to analyze and examine the failure of parameter-induced simulation crashes in climate models.

1.3 Research Objectives

The undertaking of this study follows efforts to attain the following objectives;

- Modelling of climate crashes using machine-learning algorithm using fuzzy neural networks.
- To determine if there are any crashes or failure that are associated with the use of simulation models.
- To determine chances that parallel ocean program simulation will fail.
- To develop solutions that can be used to improve climate model development and implementation.

1.4 Research Methodology

In order to reduce obstacles that are associated with ocean, ice, sea and atmospheric uncertainties that are surrounding with the model components of CCSM4. The observed failures were observed from a combination of CCSM4 and Parallel Ocean Program (POP2) simulations of perturbed parameters. The ice sea model was undertaken in conjunction with the POP2 and analyzing of the atmosphere and land elements was done using data based components. The study also involves the use of a 10 year integrated simulation and the use of normal year forcing and provides climatological air-sea data. Support Vector Machines (SVM) and Neuro-Fuzzy model (NFM) were also used to determine chances of failure of the models.

1.5 Significance of the Study

The importance and value of climate models lies in their ability to accurately and effectively fulfill their mandate. Thus by identifying challenges that may cause failure in climate models, improvements can easily be made and new, refined and better climate models can be developed. This study also offers significant value to both the academic and professional climate modelling institutions as it has to a greater extent managed to identify simulation crashes as well as problems that triggered such crashes. In addition, it can also be used as a point of reference upon which future studies can be based on. Furthermore, the frequency of crashes has been reported to be high but other cases have remained undocumented and thus this study will add to the list of documented cases of crashes of climate models.

1.6 Organization of the Study

This study is organized as follows;

- **Chapter One:** Gives an outline of this study involves looking at issues that surrounding parameter induced simulation crashes in climate models and what it hopes to achieve in the process.
- **Chapter Two:** Gives a detailed insight about climate modelling.
- **Chapter Three:** Deals with the classification of climate models by machine learning.
- **Chapter Four:** Looks at the Neuro-fuzzy model and SVM simulations methods that were employed to establish the failures, causes as well as solutions that can be used to deal with model failures and provides a detailed outline of analysis of the obtained findings.
- **Chapter Five:** Concludes the study by looking at conclusions that have be drawn, recommendations and possible suggestions to improve future studies.

CHAPTER 2
CLIMATE MODELLING

2.1 Overview

Climate models (CM) are basically considered to be apparatus that are used to enhance understanding as well the ability to predict future climate changes either on centennial, decadal, annual or seasonal time scales (Boer & Yu, 2003). A prominent example is what are termed global climate models and these are made up of a combination of mathematical equations or expressions of how sea ice, ocean, land surface and atmosphere (climate systems elements) and how they interact (Gregory et al., 2002). CMs are interlinked to how human activity, natural changes and or a combination of both provides an explanation to variations in climate conditions. The information provided by CMs is often of great importance and can be used for local, regional and even national programs and (Allen & Ingram, 2002), established that CMs are a useful tool to any nation or continent as they can be utilised for issues or policies that include among others water resources management. A notable effort towards the use of CMs has been witnessed by the development of long used Geophysical Fluid Dynamics Laboratory.

The development of CMs has also been linked with efforts to determine climate sensitivity (Murphy, 1995), and the impact of climate features (Sausen et al., 2002). This is often characterised by the use of two distinct processes and these are prognosis and, attribution and detection (diagnosis).

There is however disagreements that surround the use of CMs. For instance, Cubasch et al. (200) contend that CMs provides useful information which is also validated by other researchers and modelers through rigorous experiments which helps to curb uncertainties while Boer and Yu, (2003), outlined that CMs can be utilised to determine how changes in climate elements such as heating and cooling causes responsive effects on climate conditions. Climate models tend to differ in terms of their spatial and temporal resolution, degree of simulation and complexity. Basically climate models tend to fall into four different groups and these are;

- General circulation models tend to use discrete equations that are governed by certain surface, ocean and atmospheric laws. This study is based on the use of global climate

models (GCMs) and will address some of the core elements of the GCM which include 3-D, surface dynamics and processes, vertically resolved atmosphere and radiation balance. GCMS are often made up of a grid that stretches between 100-200km and at its surface it tends to deal with energy, water and ground temperature fluxes (Boer & Yu, 2003). GCMs can further be utilized to examine mass, momentum and energy conservation. Of most importance is the parameterization process which involves the expressing a process into an equation form and solving for the model variables so as to provide answers to the established questions (Bengtsson et al., 2006). This however requires data collected from observations under study. It is important to also note that parametrization is largely determined by the time scale. That is, certain types of parameterizations are conducive for longer time scales while others are desirable for short time scales (Yoshimura et al., 2006).

- Statistical dynamical models include an examination tool of which is a combination of energy balanced models and how energy is transferred horizontally (Sugi et al., 2002).
- Radiative-convective models tend to encompass broader simulation of energy and how it is transferred through the atmosphere (McDonald et al., 2005).
- Energy balance models involve the simulation of latitudinal and global radiation balance (Durman et al., 2001).

This chapter describes the characteristics and chaotic behaviour of climate modelling. The parameters such as temperature, precipitation, tropical cyclones and an evaluation of contemporary climate as simulated by global climate models.

2.2 Climate modeling and the Chaotic theory

One of the objective of this study is to determine what causes simulation failure and such an instance can be described by the chaotic theory which asserts that weather is chaotic (Evans & McCabe, 2010). This has implications on the study of the climate which by definition is the study of weather conditions prevailing in a certain place (Artale et al., 2010). This stems from ideas which have shown that air has low viscosity and friction and is also light and hence causes chaotic effects which affects climate simulations (Leung et al., 2003). As a result, when the wind blows, the weather is always in a state of disequilibrium. This also tends to affect the climate as well in the sense that equilibrium radiation physics is used to provide explanations to climate changes. This is accomplished by looking at changes in global temperatures (Kiehl & Shields, 2005). The

chaotic theory thus contends that predictable greenhouse gas forcing are responsible for major chaotic effects while smaller chaotic effects are considered to be due to volcanoes, sun and weather changes etc. These factors can strongly affect a simulated model as postulated by the chaotic theory. This can be supported by ideas given by Watanabe et al. (2010), which shows that climate modelling is not an easy thing as weather changes are in a strong position to cause chaotic behavior which can undermine the desired and possible outcomes. Such ideas were established by Lorenz (1963), whose work through hydrodynamics established that climate changes are characterised with non-linearity. This non-linearity is due to unpredictable air oscillation behavior and this can be illustrated by figure 2.1.
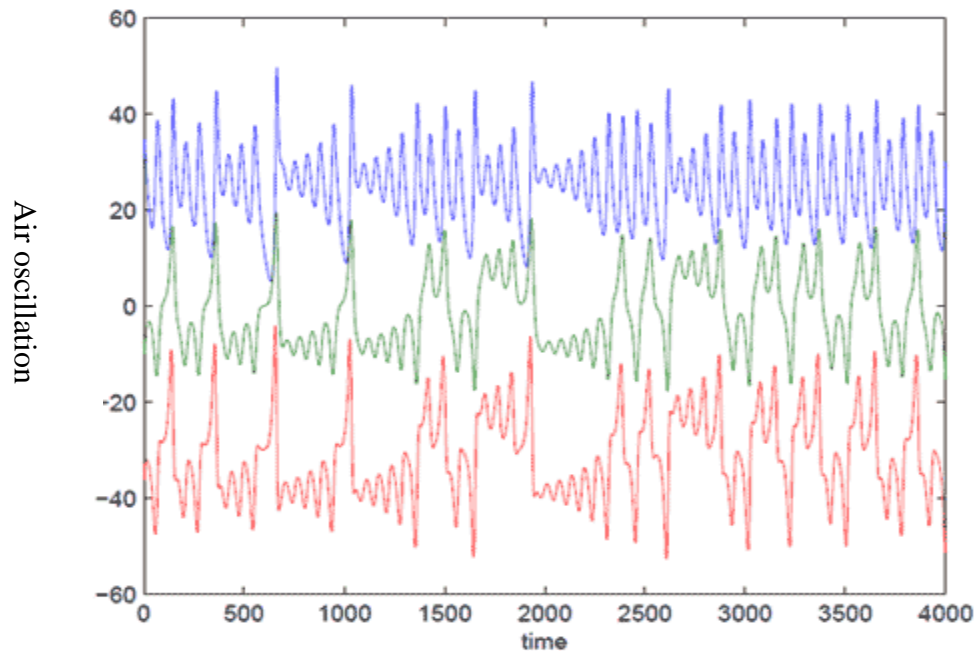
Figure 2.1: Lorenz phase space equations of air convection, Lorenz (1963)

Figure 2.1, illustrates that small climate changes are bound to have unpredictable outcomes and this implies that climate model simulations can fail in the event that these small climate changes have posed huge unpredictable outcomes. When climate change is highly associated with unpredictable outcomes simulation can be difficult and bound to fail (Watanabe et al., 2010).
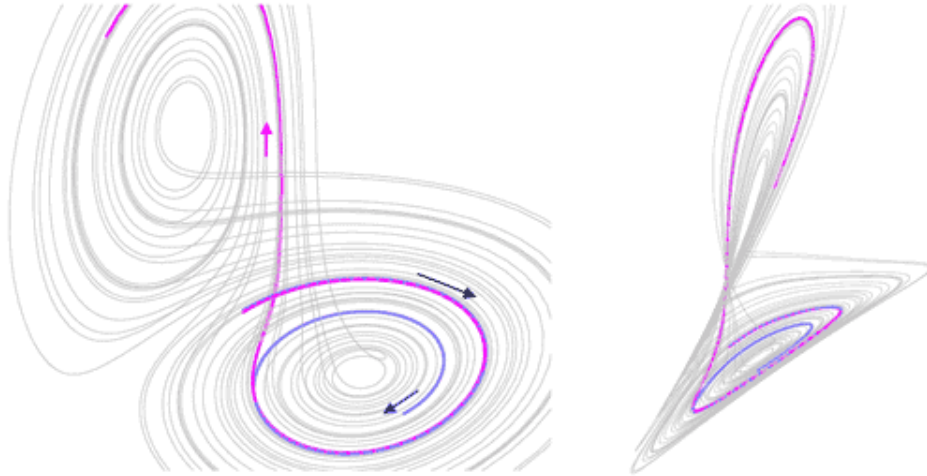
Figure 2.2: Illustration of deterministic chaos, Lorenz (1963)

Figure 2.2, is based on the idea that two weather systems or patterns with initial conditions are bound to follow similar patterns for a certain period of time. The Lorenz attractor thus shows that after a certain period of time, the ability to accurately predict them will fall. This is what most scholars claim that climate modelling is associated and affected with unpredictable outcomes (Kiehl & Shields, 2005; Leung et al., 2003; Watanabe et al., 2010). Such is supported by Evans and McCabe (2010)) who established that oceanic indices also have smaller chaotic influences, Artale et al. (2010), contends that air and water have different Rayleigh numbers with that of air being greater than that of water and hence water cannot is difficult to ascertain its chaotic influence in ocean currents while McDonald et al. (2005), established that a lot of climate changes are due to heat transfers which can pose chaotic influences of climate simulations.

Just like simulation failure, the chaotic theory predicts that chaotic weather behavior and outcomes is surrounded with some level of uncertainty which declines with time (Kiehl & Shields, 2005). This therefore implies that the extent to which a simulation model will fail also tends to decline with time. This can be supported by ideas given by Watanabe et al. (2010), which showed that simulation model tend to improve with time and hence simulation failures tends to decline with improvements made. Furthermore, the chaotic theory of climate change tends to posit that chaotic behavior can be determined with equations (Artale et al., 2010). Such is the same with simulation failure and equations can be used to determine whether a climate simulation model will fail. This can include things such as probability and algorithms to determine both chances success and failure.

Thus the chaotic theory was employed in this study to offer a sound base about what causes simulation failure, determine the chances of a simulation model succeeding or failing, what can be done to determine the probability of simulation success and failure, and what can be done to improve simulation success. Alternatively, it can be said to highlight the importance of uncertainty when developing simulation model, the use of mathematical equations (probability and algorithms) to conduct climate simulation and the importance of model improvement in dealing with simulation failure (chaotic outcomes).

2.3 Model simulation Extremes

Extremes have been observed to be dominating climate change headlines in terms of severity and frequency. This stems from concerns which have been raised by most scholars citing that climate change and variability have increased especially on a high note (Durman et al., 2001). Problems have been noted when simulation models were failing to capture these extremes and hence forcing model improvements that can address such concerns (Kiktev et al., 2003). However, improvements in dealing the simulation of extremes have been made following the introduction of new indices and data availability (Yoshimura et al., 2006).

When dealing with extremes, it is important to note that not all extremes are the same because others take place due to local instabilities, higher altitudes or rapid amplification (Bengtsson et al., 2006), have short duration (Sugi et al., 2002) and are smaller in scale (McDonald et al., 2005). Long lasting and large scale extremes are most cases caused by continuous weather events that are linked with land-air and sea-air interactions. But temperature extremes have been well simulated by prevailing models and this is made possible by analyzing tropical cyclones, frequencies and precipitation intensity, minimum and maximum temperatures amplitudes etc. That of precipitation is conducted by looking at its extreme precipitation rates.

2.3.1 Extreme Temperature

Flowing comparisons of Hadley Centre Atmospheric Model version 3 simulations done by Kiktev et al. (2003), it was noted that temperature extremes were mainly as a result of anthropogenic radiative forces. Such is considered to occur when the number of frost days is declining and at large spatial scales (Kiktev et al., 2003). Meehl et al. (2004), outlined that poor simulations can be made when the number of warm nights is not captured correctly and that by including anthropogenic forcing, model trend features can be improved to a greater degree. This can be

supported by observations made by Meehl and Tebaldi (2004), which showed that a 2 days decline in frost days is evident when greenhouse, ozone, sulphate aerosol, volcano and solar variations are included in the simulation process. However, such results tend to differ with the region or place in which the simulations have been made (Meehl et al., 2004). Following AMIP-2 precipitation extremes done by Kharin et al. (2005), it was discovered that warm temperature extremes are in most cases well simulated. On the other hand, Vavrus et al. (2006), established that the magnitude and location of cold air breaks will be prevalent in those prevailing climate conditions. Studies have also be done to examine the association between heat waves or cold air breaks and large scale air breaks. For instance, it was discovered that for precipitation that exceeds 10mm and downstream, cold breaks are more likely to be high (Vavrus et al., 2006) while observations have shown that a 500hPa circulation heat wave was common over North America and Europe (Meehl and Tebaldi (2004).

2.3.2 Extreme Precipitation

Following investigations that have been made by Sun et al. (2006), involving 18 AOGCM simulations, heavy events have been noted to be having little precipitation which is less than 10mm a day. Community Climate Model version 3 by Iorio et al. (2004), have also showed that accurate and real precipitation results are obtainable for high resolution simulations. This can be backed by examinations conducted in Japan and the established results by Kimoto et al. (2005), confirmed this to be true. The results still point to the same view though different simulations models have been used in each extent. For instance, cases involving the use of HadCM2 GCM found the same results (Durman et al., 2001) and where a HadAM3 by Kiktev et al. (2003) was used the same conclusions were made. Conclusions under this instance can therefore be made that simulation models must be in a strong position to accommodate extremes and the best way to do that is by including anthropogenic forcing.

2.3.3 Tropical Cyclones

Not all models can simulate tropical cyclones and Oouchi et al. (2006) contend that the intensity of such climate events is high and this makes it difficult for certain models to simulate them. Thus, running on a high resolution an SST boundary method has been established to offer better improvements and efforts towards the simulation of tropical cyclones (Camargo et al., 2005). But ECHAM5s have been in a strong position to produce better hemispheric or tropical global metrics

of tropical cyclones (Allen & Ingram, 2002). Despite the presence of such tools, errors have been noticed in some simulated models and are normally high when the intensity and frequency of tropical cyclones is very high (Meehl et al., 2004). This can be augmented by ideas given by Cubasch et al. (2001), which posit that the simulation of tropical cyclones is also associated with high sensitivity of conventional parameterization. Thus a proper tropical cyclone simulation requires high resolution models. This can even result in good simulation even if parameterization is not undertaken but so long as large convective systems are present.

2.4 Evaluation of Contemporary Climate as simulated by Coupled Global Models

Spelman and Manabe (1984), established that the response of a climate system tends to vary and this is due to nonlinearities that surround the climate. Thus, the ability of a climate model to accurately offer climate forecasts is determined by the extent to which prevailing climate conditions are simulated together with the undetermined level of fidelity. Modelling difficulties exist either because of lack of knowledge, skills, experience or information etc., can pose challenges in simulating prevailing climate conditions. This can also imply that dynamic of physical misspecification of processes (Sausen et al., 2002). Hence, Delworth et al. (2006), contends that climate models that are capable of simulating diurnal and seasonal cycles, and difficult spatial conditions, the greater the assurance that all the concerned elements have been covered or addressed. This was further supported by Collins et al. (2006), citing that the effectiveness of any developed model is determined by its ability to simulate present climate conditions. A multi-model mean field is often used to determine model bias and can deal with errors that considered to be pervasive. But climate characteristics are more likely to affect the accuracy of models in simulating climate changes. These elements do not only affect the ecosystem but also the society and can have a high responsiveness to radiative forcing. These characteristics are herein discussed as follows;

2.4.1 Ocean

The ocean is also another variable which plays an important role which determines the climate models respond transiently. Thus it can be said that ocean elements or characteristics do pose an effect on climate response. This can be evidenced by ideas given by Gregory et al. (2002), which clearly indicated that oceanic simulation's fidelity is largely influenced by surface fluxes. This is because oceanic simulation is directly impacted by both the ocean and the atmosphere. Modelling

problems can sometimes arise because water and surface heat fluxes are deduced from information provided by other population samples and hence can be difficult to observe sometimes (Boer & Yu, 2003). This is also affected by the problem that the observed estimate is surrounded by a lot of uncertainties. This therefore requires that models look at the ocean's horizontal transports (Yoshimura et al., 2006).
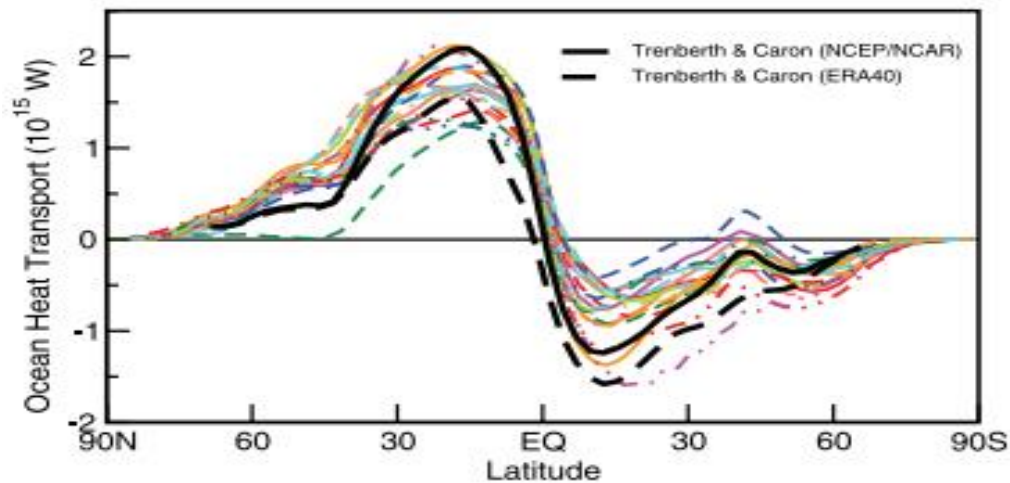
Figure 2.3: Ocean heat transport, Durman et al. (2001)

Figure 2.3, depicts that a lot of models that are simulated do transport large amounts of heat towards the north and this tends to differ with cases that involve estimates made from observations. This is also similar to ideas that have been made by Ganachaud and Wunsch (2003), which showed that at the 0.6×10^{15} model simulations are more concentrated at 45°N. However, as one moves from the equator, a lot of observations will be highly concentrated between or within observation depicted in figure 2.3.

2.4.2 Atmosphere

It is important to note that models that can correctly capture all the processes are those that can deal with compensating errors accurately simulate surface temperatures of diurnal and annual cycles (Bengtsson et al., 2006). This is supported by ideas given by the study by (McDonald et al., 2005), which showed that either energy movements caused by the ocean or atmosphere is necessitated by surface heat fluxes, clouds and insolation distribution. Moreover, diurnal and annual surface temperature cycles are also determined by diurnal and annual variations. However,

the extent to which soil and upper ocean layers store energy tends to affect these variations. Atmospheric influences will pose effects on simulation in two ways and this are;

2.4.2.1 Temperature

Temperature differences are usually noted among different climate models and a study by Kiktev et al. (2003), exhibited that large models are more prone to huge errors. This was also supported by observations made by Durman et al. (2001), which showed that at lower attitudes, temperatures errors can reach as high as 3°C for individual models. The extent to which errors occur as well as the magnitude of errors made has been established to vary with the region in which simulation has been made (Sugi et al., 2002). This can be supported by ideas given in figure 2.1, which shows that differences between the actual topography and the smoothed model topography can have sharp elevations which cause huge errors.

Cold biases are also a common element that can affect climate model simulation but under this case such bias might be insignificant. Towards the eastern tropical basins, huge errors are also likely to be evident and this is as a result of having low clouds simulations (McDonald et al., 2005). However, a study by Durman et al. (2001), established that the magnitude of effect posed on external perturbations by systematic model errors is to some extent very low.
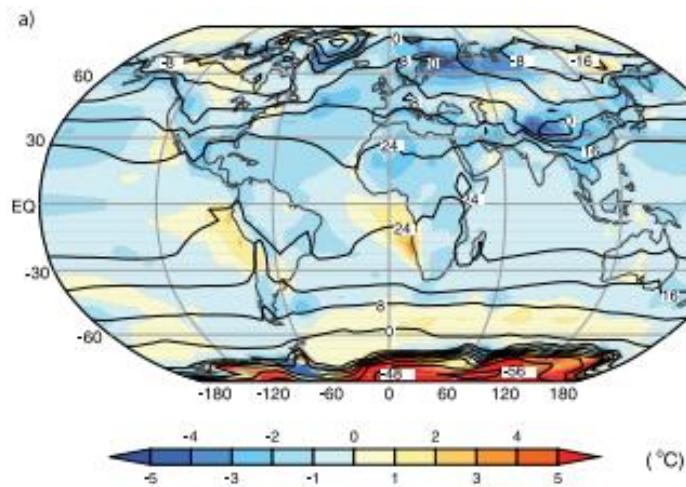
(a) Climatological annual mean SST,
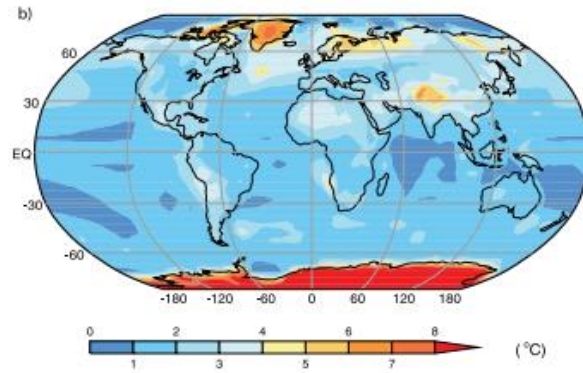
(b) Size of the typical model error, as gauged by the root-mean-square error

Figure 2.4: Typical model errors and observed climatology, (Rayner et al., 2003)

From figure 2.4, observations can be made temperature errors do not exceed 2°C in regions that do not have accurate data or have poor data and those not in the polar regions tend As noted from figure 2.4, SST and surface air temperature experienced over the land are prime determinants of the recorded average surface temperatures. Figure 2.4, also shows that there are significant differences between the observed field and the multi-model mean field.

Meanwhile, though these errors can affect climate mode simulations, climate models have been established to provide major explanations of global temperature patterns (Kimoto et al., 2005). Lorio et al. (2004), contend that recorded spatial patterns of mean temperatures are correlated with simulated mean temperatures and is close to 1. This points to the idea that the fidelity of models does govern the climatology of surface temperatures.
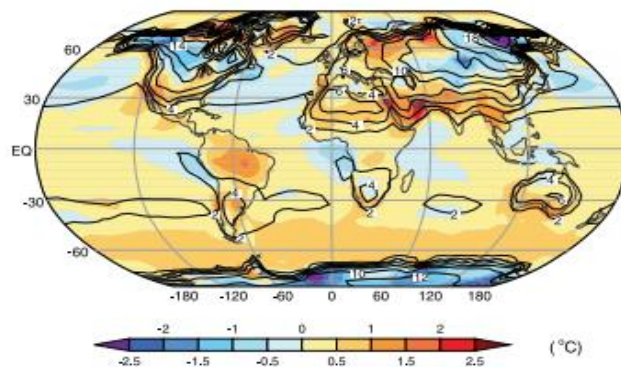
Figure 2.5: Recorded standard deviation of SST over surface air temperature and land, Rayner et al. (2003)

On the other hand, the effectiveness and accuracy of a model can be determined by looking at the recorded surface temperature cycles. This is denoted in figure 2.5, and it shows that variations in monthly average monthly surface temperatures is due to semi-annual and annual elements of the annual cycle. Figure 2.5, also shows differences that have been noted between observations' mean and that of the model. The importance of this diagrammatic model is that model errors are within the 2°C limit for every 10°C change in surface temperature. These given models do accommodate variations between continental and maritime environments.

2.4.2.2 Balance of Radiation

It is noted by Vavrus et al. (2006), that at the upper atmosphere the local differences between long wave radiation and shortwave radiation is attributed to seasonal and latitudinal changes in the incidence of the sunlight. Thus things like surface characteristics and the distribution of the clouds can impact insolation distribution. Observations do point that at the poles, annual mean insolation tends to be lower as compared to the tropics (Bengtsson et al., 2006; McDonald et al., 2005; Sugi et al., 2002). This implies that radiation imbalances have strong implications on climate simulation and errors can be high as differences in these two climate characteristics are factored in. thus models which does not cover these aspects are more likely to be mis-specified.

2.4.3 Land Surface

One of the challenges that can be encountered towards climate simulation especially of the land surface is inadequate observations. Kattsov and Källén (2005) noted that modelers can sometimes fail to obtain the necessary and sufficient observation to conduct land surface simulations. Things such as momentum and carbon fluxes, frozen or melting snow, drying and logged water and surface albedo can have a huge interplay on the distribution of energy between latent heat and sensible fluxes. Thus not all climate models can be analyzed on long or spatial temporal scales (Bengtsson et al., 2006). It also important that when conducting simulation, climate models must cover things such as surface fluxes, carbon and land hydrology.

2.4.4 Sea Ice

It is well established that sea ice features have huge effects on spatial and magnitude influence of high latitude climate variations (Arzel et al., 2006; Walsh et al., 2002). Insufficient observations of things such as the thickness of the ice. Bitz et al. (2002), contends that though some sea ice errors are measurable, they are to a large extent difficult to separate what causes them. Among the

probable reason is the idea that the extent to which sea ice is captured might not be that sufficient to adequate enough (Kattsov & Källén, 2005). Other ideas do point that at high latitudes, simulations errors in oceanic and atmospheric elements can trigger movements in ice (Walsh et al., 2002). Thus, it can therefore be established that climate models that can effectively simulate climate changes must capture seasonal variations of sea ice (Kattsov & Källén, 2005). A lot of simulation bias of sea ice made by models is with respect to high latitudes (Holland & Bitz, 2003). There are also other errors that climate model simulations can suffer from in this respect and this includes heat flux errors. Poor atmospheric parameterization and failure to simulate high-latitude cloudiness (Arzel et al., 2006).

2.4.5 Changes in model Performance

Inter-comparison of models has of lately been made possible by the use of standard experiments which provided results that can track the models' historical performance. Among such are Coupled Model Inter-comparison Project (CMIP1&2) and MMD. Thus model output helps to express changes in model performance into quantifiable means using the 14 groups that have been providing model outputs (Circa, 2000). Information about sea level pressure, precipitation, and surface temperature can be provided through CMPIPI & 2 monthly fields. This helps to determine the performance of simulation models but CMIPI & 2, and the 20th century MMD simulations features are not identical (Lorio et al., 2004). The probability of climate models such as global models to simulate climate changes can depicted by figure 2.6.
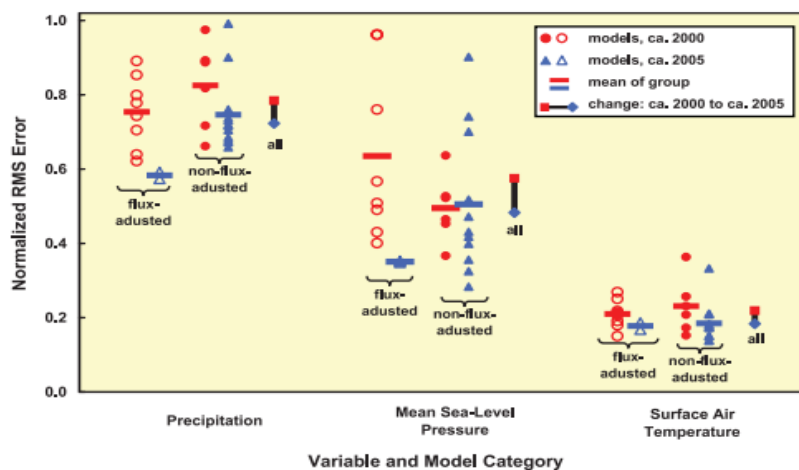
Figure 2.6: Normalized RMS error in simulation of climatological patterns, Kiktev et al. (2003)

Figure 2.6 shows the extent to which models can accurately determine surface temperature, sea level pressure and precipitation simulations in comparison to this that have been made in the past. After the twelve climatological months, the RMS error can easily be computed for the whole globe and it is used to analyse the combined effects of seasonal cycle and spatial pattern errors (Kimoto et al. (2005). Figure 2.6, also denotes that temperature simulation is at its best while precipitation is less simulated that pressure. It can also be noted that flux adjusted models tend to have better mean errors. These results do confirm that current models that are now being used for simulation can to a large extent perform well in climate modelling.

CHAPTER 3

MACHINE LEARNING APPROACH FOR MODELLING CLIMATE CRASHES

3.1 Overview

This chapter presents machine-learning algorithms used for climate modelling. The chapter also gives a description of the design of NFM and SVM algorithms and how they will be used to predict simulation failure.

3.2 SVM Classification

SVM is a machine learning algorithm that is used to build models, analyze data and deal with classification challenges (Joachims, 1998). Alternatively, it can be known as a combination of various coordinates of a particular observation (Zeng, 2008). The concept of SVM is built on the idea and need to choose the best hyper-plane on the basis of accurate classification and maximization of margin. The use of SVM is also supported by kernel functions which help to transformation of dimensional input space (from low to high dimensional space). One good aspect of SVM is that model parameters can be tuned so as to enhance the performance of the model (Scholkopf & Smola, 2001). Just like any application, the use of SVM is characterized by both benefits and cons and such are outlined as follows;

- It perfectly incorporates the idea of margin of separation.
- Effectiveness in high dimensional spaces is always high when
- It is also compatible with situations that are characterized by that has a mismatch between the samples and dimensions (sample size is greater than the number of dimensions) and the sample size.
- It can also be considered to be efficient in terms of memory and this is due to the fact that it uses support vectors in dealing training points.

The SVM approach has been criticized on the basis that it is incapable or ineffective to handle large data sources which a lot of training (Zeng, 2008). Joachims (1998) outlined that the performance of SVMs is limited and is high when the situation requires a lot of training. In addition, its use is also surrounded by the idea that it does not offer direct probability estimates (Scholkopf & Smola, 2001).

Given an input vector a, simulations can be assigned to classes K_S and KF using SVM, that is, support vector machines (Bishop, 2007). There are also several methods that can be utilized to assign such classes and these include random forests (Hosmer & Lemeshow, 2000), decision trees (Bishop, 2007), neural networks decision trees (Breiman et al., 1984), and logistic regression (Breiman, 2001). Due to the nature of performance and feasibility in the use of algorithms, this study however concentrated on SVMs.

The SVM approach caters for misspecifications from the soft margins (overlapping data) by maximizing the margin area that exists between the classes. For classes that are separable and are linear, greater dimensional features can be obtained through the transformation of input spaces. Kernel functions provide an easy way of transforming input spaces as denoted by figure 3.3. On and within the margin of the classes, separable training points can be found there and these are known as support vectors (Gent & McWillimas, 1990). The predictive decision function can be used to assign a new input vector x.

$$f(x) = \sum_{n=1}^{N_s} y_i \beta_i K(xi + x) + b \qquad (3.1)$$

The SVM follows ideas which were developed by Vapnik and improvements were later made by Cortes and Vapnik (1995) and they emphasis was to determine the hyperplane with the optimum separation with the longest distance between data points. Given (X_i, Y_i) data points of a binary classification with classes $Y_i \in -\{1,1\}$ and $Xi \in R^P$ and all the vectors are denoted by (X_i). The two points can be divided in to classes by a maximum margin hyperplane and this can be expressed as follows;

$w.x + b = -1$ and $w.x + b = 1$ \qquad (3.2)

In this case the normal vector of the plane will be represented by w and it tries to stop data from falling into margin by minimizing ||w|| by incorporating a constraint for Xi of the second class or $w.x_i - b \leq -1$ for X_i or w. xi - ≥ 1 for i. samples along the vector hyperplanes are what is known as Support Vectors (SVs) which are described by M= $\frac{2}{||w||}$ which offers insights about training data. The optimization quadratic problem can be applied in this case as follows;

Maximize ||v||

Subject to ym(v. xm – b $\geq$1 for any m=1, ...n

Huge emphasis in SVM is to minimize the error and maximize the margin of operation of the training error. We can thus apply Langrage multiplier to the aforementioned expression which results in the following expression;

$$\max imize \quad L(\alpha) = \sum_{i=1}^{n} \alpha_i - \frac{1}{2} \sum_{i,j=1}^{n} y_i y_j \alpha_i \alpha_j K(x_i, x_j)$$

$$subject \ to \quad \sum_{i=1}^{n} y_i \alpha_i = 0$$

$$\alpha_i \geq 0, \quad i = 1,...,n.$$

The kernel function that satisfies the Mercer theorem is given by $K(xi, xj) = (\varphi(xi), \varphi(xj)$. The best optimal solutions are required to meet complementarity conditions established by the Karush Kuhn Tucker (KKT).

$$\alpha*_i [y(w* \varphi(xi) + b *) - 1 = 0, i = 1, ... n.$$

The solution of the dual problem will be given by $\alpha*_I$ which gives rise to the following SVM function;

$$f(x) = sgn(\sum_{i=1}^{m} \alpha_i^* y_i K(x_i, x_i^*) + b)$$

(3.3)

The number of support vectors is given by m. the SVM can thus be considered to be an essential tool which is used deal with supervised classification issues and this is made possible because of its generalization ability.

Given an input vector a, simulations can be assigned to classes K_S and K_F using SVM, that is, support vector machines (Bishop, 2007). There are also several methods that can be utilized to assign such classes and these include random forests (Hosmer & Lemeshow, 2000), decision trees (Bishop, 2007), neural networks decision trees (Breiman et al., 1984), and logistic regression (Breiman, 2001). Due to the nature of performance and feasibility in the use of algorithms, this study however concentrated on SVMs.

The SVM approach caters for misspecifications from the soft margins (overlapping data) by maximizing the margin area that exists between the classes. For classes that are separable and are linear, greater dimensional features can be obtained through the transformation of input spaces. Kernel functions provide an easy way of transforming input spaces as denoted by figure 3.3. On

and within the margin of the classes, separable training points can be found there and these are known as support vectors (Gent & McWillimas, 1990). The predictive decision function can be used to assign a new input vector x.

$$f(x) = \sum_{n=1}^{N_s} y_i \beta_i K(xi + x) + b \qquad (3.4)$$

With Eq. (4), CS and CF have respective values of $f(x) < 0$ and $f(x) > 0$, langrage and bias multiplier are denoted by b and β, kernel function $k(x_i + x)$, indicator variable of a binary outcome $y_i \in \{-1,1\}$ and support vectors N_S. Constrained optimization is used to ascertain both the langrage and bias multiplier as taken from Chang and Lin (2011). The challenge with Eq. (1) is that it does not an indication of the probability of class membership. As a result, this study had to make extensions to the SVM method. This can be made possible by the use of cross validation and training data that establishes a two parameter expression by introducing λ to equation 2 (Chang & Lin, 2011). Thus, in order to calculate the probability of failure $P(K_f /x)$, LIBSVM was used. The study also developed a category of SVM classifiers using an ensemble strategy (Dietrich, 2000). Outcomes are obtained for each category and they are in turn utilized to determine how the system performs and simulation failures.

3.3 Neuro-Fuzzy model for Structure Identification

Neuro-Fuzzy model is a combination of neurace and fuzzy systems which is used to deal with pattern recognition, prediction, identification and control problems. Fuzzy sets are in two types, type I and II fuzzy sets but the type II was established out of type I fuzzy set (Lamarque et al., 2013). In the thesis, type I fuzzy sets is applied for the design of NFM model. They use of Gaussian membership functions characterized by width and center parameters.

$$\bar{\mu}(x) = \exp\left(-\frac{1}{2}\frac{(x-c)^2}{\sigma^2}\right) \qquad (3.5)$$

The input vector X, width and center of the membership function are denoted by m and σ, Correspondingly.

The Neuro-Fuzzy model (NFM) realize the fuzzy reasoning process through the structure of neural networks. Here, it is necessary to determine the accurate of the Neuro-Fuzzy model. This is obtained through evaluation of the error response of the designed classification system. TSK type

fuzzy rules are basically used for designing the fuzzy systems. TSK fuzzy rules include fuzzy antecedent and crisp consequent parts. These fuzzy systems approximate nonlinear systems with linear ones and have the following form:

If x_1 is A_{11} and x_2 is A_{21} and ... and x_m is A_{m1} Then $y_1 = b_1 + \sum_{i=1}^{m} a_{i1} x_i$

If x_1 is A_{12} and x_2 is A_{22} and ... and x_m is A_{m2} Then $y_2 = b_2 + \sum_{i=1}^{m} a_{i2} x_i$

$$...$$ (3.6)

If x_1 is A_{1n} and x_2 is A_{2n} and ... and x_m is A_{mn} Then $y_n = b_n + \sum_{i=1}^{m} a_{in} x_i$

Here x_i is input and y_j is output signals of the system, $i=1,...,m$ is the number of input signals, $j=1...r$ is number of rules. A_{ij} is input fuzzy sets, b_j and a_{ij} are coefficients. The structure of (NFM) used for classification of liver disorders is given in Figure 3.1. The (NFM) consists of six layers. In the first layer, the x_i $(i=1,...,m)$ input signals are distributed. The second layer is membership functions that describe the linguistic terms. Here, for each input signal entering the system, the membership degree to which input value belongs to a fuzzy set is calculated.
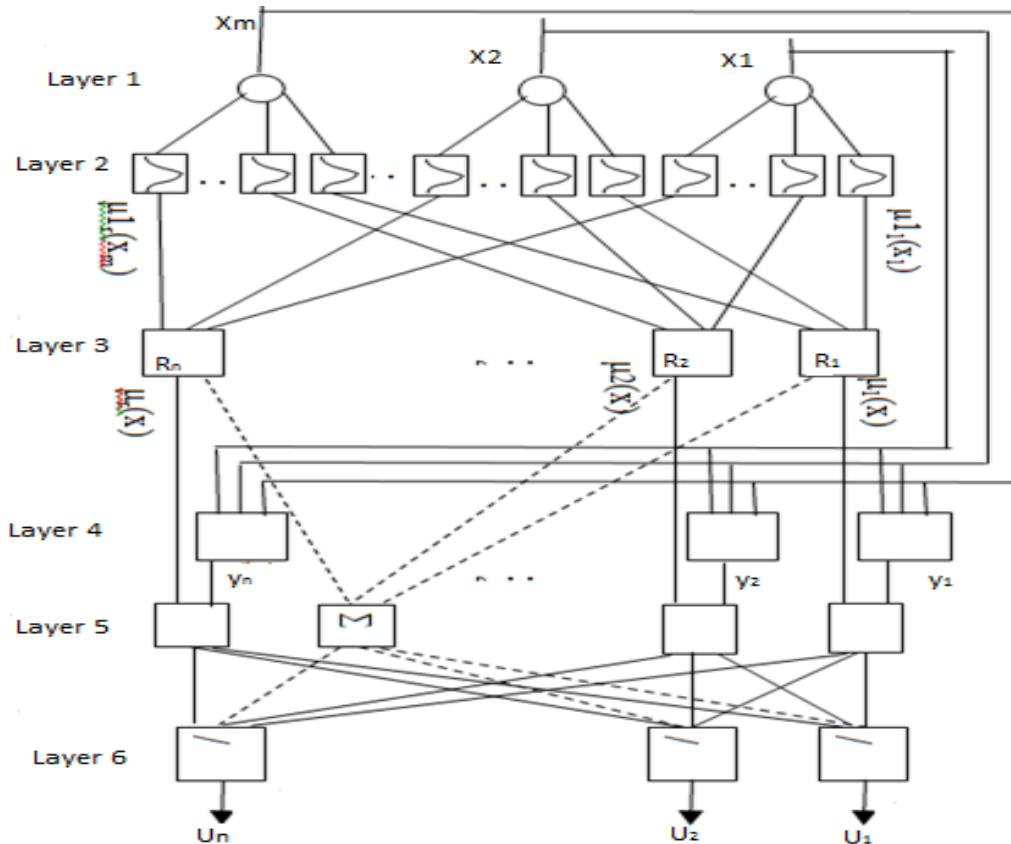
Figure 3.1: Topology of the proposed NFM

The third layer is a rule layer. Here number of nodes is equal to the number of rules. $R_1, R_2, ..., R_r$ represents the rules. The output signals of this layer are calculated using t-norm min (AND) operation:

$$\mu_j(x) = \prod_i \mu 1_j(x_i) \,, \; i=1,..,m, \; j=1,...,r \tag{3.7}$$

where Π is the min operation. These $\mu_j(x)$ signals are input signals for the fifth layer. Fourth layer includes n linear systems. Here the values of rules output are determined.

$$y1_j = b_j + \sum_{i=1}^{m} a_{ij} x_i \tag{3.8}$$

In the next fifth layer, the output of j-th node is calculated as:

$$y_j = \mu_j(x) y1_j \tag{3.9}$$

The output signals of FNS are computed in the sixth layer

$$u_k = \frac{\sum_{j=1}^{r} w_{jk} y_j}{\sum_{j=1}^{r} \mu_j(x)} \tag{3.10}$$

where u_k are the output signals of the networks, $(k=1,..,n)$. After calculating the output signal, the training of the parameters of the network starts.

3.4 Learning of Neuro-Fuzzy Model

Training of NFM is carried out using gradient descent algorithm. For this purpose on the output of NFM the error is determined.

$$E = \frac{1}{2} \sum_{p=1}^{O} (y^d - y)^2 \tag{3.11}$$

Current and desired output are given by Y^d and Y while the number of training samples is given by O for an input vector p. Here n is the number of output signals of the network, desired output is u_k^d and u_k the current output values of the network ($k=1,..,n$). The parameters are w_{jk}, a_{ij}, b_j, ($i=1,..,m,\ j=1,..,r,\ k=1,..,n$) and c_{ij} and σ_{ij} as membership function. Model parameters will be adjusted by employing the following function;

$$w_{jk}(t+1) = w_{jk}(t) - \gamma\frac{\partial E}{\partial w_{jk}} + \lambda(w_{jk}(t) - w_{jk}(t-1));$$

$$a_{ij}(t+1) = a_{ij}(t) - \gamma\frac{\partial E}{\partial a_{ij}} + \lambda(a_{ij}(t) - a_{ij}(t-1));$$

$$b_j(t+1) = b_j(t) - \gamma\frac{\partial E}{\partial b_j} + \lambda(b_j(t) - b_j(t-1));$$

(3.12)

$$c_{ij}(t+1) = c_{ij}(t) - \gamma\frac{\partial E}{\partial c_{ij}} + \lambda(c_{ij}(t) - c_{ij}(t-1));$$

$$\sigma_{ij}(t+1) = \sigma_{ij}(t) - \gamma\frac{\partial E}{\partial \sigma_{ij}} + \lambda(\sigma_{ij}(t) - \sigma_{ij}(t-1));$$

$$i = 1,...,n;\ \ j = 1,...,r;\ \ k = 1,...,n.$$

With $i=1,...,m; j=1,...,r; k=1,...,n.$

Here m is the number of input signals and r is the number of fuzzy rules , γ is the learning rate, and λ is the momentum.

CHAPTER 4
SIMULATION

4.1 Overview

This part outlines methodological steps that were carried out with efforts to provide answers to the established research questions. Deduced conclusions as well as given recommendations are based on the results that were obtained following these given procedures. Thus this chapter with look at research methodology, how the ensemble simulations are to be conducted, the adopted descriptive and probabilistic failure analysis SVM classification and Neuro-Fuzzy model. These steps are herein discussed in details.

4.2 Simulation Design

The study is based on developed POP2 models which made it easy to select ocean model parameters that were used in this study. These model parameters were subjected to different parameterizations on a sub-grid scale and this was done six times. The main emphasis behind such parameterization was to determine the resultant outcome of vertical and horizontal oceanic turbulent after simulation. Table 4.1 provides details of the uncertainty ranges of the model parameters used in this study.

Spatial anisotropic viscosity was used to ascertain the horizontal momentum and was represented by the parameters 13 to 18 in line with formulations established by Smith and McWilliams (2003), while isopyenal eddy-induced transport of the horizontal mixers were for parameters 10 to 12 and these were established from a study by Gent and McWillimas (1990). Information established by Fox-Kemper et al. (2008) outlined that parameters 7 to 9 can be used to simulate mixed layer eddies and submesoscale while prescribed formulations by Jayne (2009), were used for the abyssal tidal mixing. Further prescriptions by Large et al. (1994), were K-profile parameterization associated with vertical mixing and convection and these corresponded to parameters 1 to 6.

Table 4.1: CCSM4 ocean model parameters

	Description	Module	Scale[1]	(low, default, high)	Parameter[2]
1	Ration of background diffusivity and vertical viscosity	Vmix_kpp	Log	(4.0, 10.0, 20.0)	Prandt1
2	Max PSI induced diffusion	Vmix_kpp	Log	(0.1, 0.13, 0.5)	Bckgrnd_vdc_psim
3	Equatorial diffusivity	Vmix_kpp	Log	(0.01, 0.01, 0.5)	Bckgrnd_vdc_cq
4	Banda sea diffusivity	Vmix_kpp	Lin	(0.5, 1.0, 0.5)	Bckgrnd_vdc_ban
5	Base background vertical diffusivity	Vmix_kpp	Log	(0.032, 0.16, 0.8)	Bckgrnd_vdc1
6	Mixed diffusion coefficients	Vertical_mix	Log	$(1.0, 10.0, 50.0) \times 10^3$	Convect_corr
7	Convect_visc (momentum) and convect_diff (tracer)	Tidal	Log	$(2.5, 5.0, 20.0) \times 10^4$	Vertical_decay_scale
8	Tide induced turbulence's vertical decay scale	Tidal	Log	(25.0, 100.0, 200.0)	Tidal_mix_max
9	Tidal mixing threshold	Mix_submeso	Lin	(0.05, 0.07, 0.01)	Efficiency_factor
10	Submesoscale eddies' efficiency factor	Hmix_gm	Log	(0.05, 0.03, 0.03)	Slm_corr
11	Slm_r (redi terms) and slm_b bolus' maximum slope	Hmix_gm	Lin	$(2.0, 3.0, 4.0) \times 10^7$	Ah_bolus
12	Bolus mixing's diffusion coefficient	Hmix_gm	Lin	$(2.0, 3.0, 4.0) \times 10^7$	Ah_corr
13	Ah_bkg_srbl (horizontal diffusivity within the surface boundary) and Ah (redi mixing's diffusion coefficient and background)	Hmix_aniso	Lin	(30.0, 45.0, 60.0)	Vconst_7
14	Variable viscosity parameter	Hmix_aniso	Lin	(2, 3, 5)	Vconst_5
15	Variable viscosity parameter	Hmix_aniso	Log	$(0.5, 2.0, 10.0) \times 10^{-8}$	Vconst_4
16	Variable viscosity parameter	Hmix_aniso	Lin	(0.16, 0.16, 0.02)	Vconst_3
17	Variable viscosity parameter	Hmix_aniso	Log	(0.25, 0.5, 2.0)	Vconst_2
18	Variable viscosity parameter	Hmix_aniso	Lin	$(0.3, 0.6, 1.2) \times 10^7$	Vconst_corr

[1] Logarithmic and linear scales were applied for parameters whose ratios were between the range high/low ≥ 5 and high/low <5, [2] individual correlated pair of parameters were denoted by numbers 1, 7, 9 and 13

4.3 UQ Ensembles and Sampling Procedures

The examination of the ensembles was done in three different stages with simulations amounting to 180. Table 4.2 provides details of such simulations as well as the success rates of each study. The first and second studies were used to program machine learning algorithms so that they can track and analyze simulation crashes. The third study was conducted so as to determine their potential to forecast simulation crashes. Table 4.2 also shows the rate of failure of the entire simulations that were done and reports that 46 failures were observed out of the 540 simulations that were done. The recorded failures were observed at different intervals of the integration phase. 18 POP2 parameter values were examined using a Latin hypercube method. This was also important as it resulted in the establishment of an ensemble. In addition, normalized log uniform probability functions were also employed to represent the model parameters' high and low values.

The adoption of the Latin hypercube method in this study is based on its reduction capabilities which are usually lower in than that of the Monte Carlo method (Davis, 2003). Meanwhile, the Latin hypercube method is an uncertainty and UQ analysis method that compromises of the Monte Carlo variant, space filling and stratified aspects (Stein, 1987). N intervals were obtained from the splits of all the D parameter distributions of the Latin hypercube, giving an ensemble size of N. thus in this study, N = 180 and D = 18.

Table 4.2: Conducted Latin hypercube studies

Study	Failures	Failure rate	Successes	Total simulations
First	20	11.1%	160	180
Second	12	6.7%	168	180
Third	14	7.8%	166	180
Total	**46**	**8.5%**	**494**	**540**

Parameter values were randomly selected from various bins by carefully ensuring that each interval is subjected to sampling once at every parameter dimension. For instance, a possible outcome out of the 120 possibilities given 2 parameters whose bins will contain indices like (5,1), (4,3), (3,5), (2,2) and (1,4). This is known as a 5-pair or 5-element Latin hypercube ensemble. Figure 3.1

provide a description of the Latin hypercube sample areas of the 3 ensembles that are used in this study.
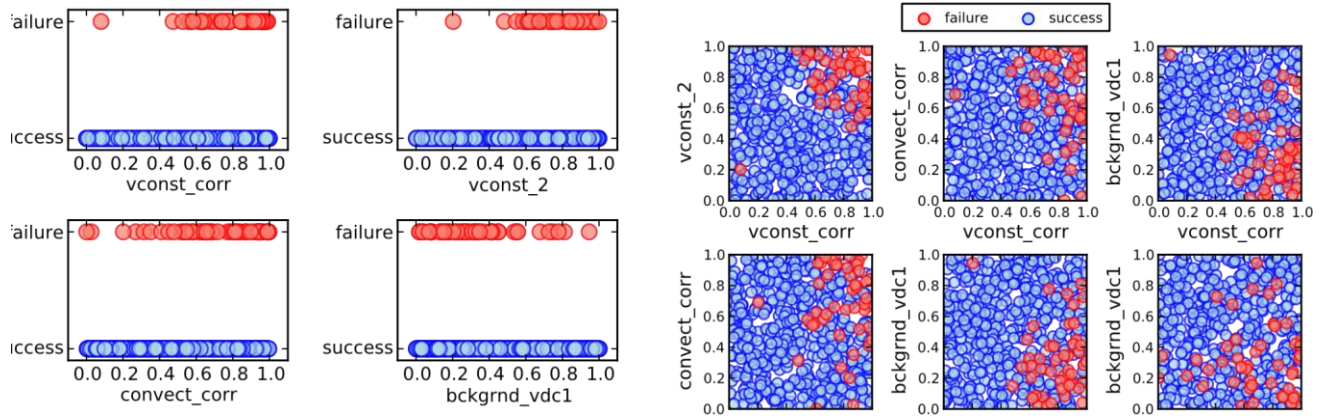
Figure 4.1: Latin hypercube sample areas of the study ensembles

It can be established from figure 4.1 that dense and uniform features are evident in the Latin hypercube. The Lawrence Livermore National Laboratory UQ Pipeline was utilized to generate the ensembles. This technique that runs on high performance computers and is used to analyze work flow systems using a Python system (Tannahill et al., 2011). According to Forester et al. (2008), such an apparatus is important as it can be used to develop surrogate models for approximating ensemble output and offers a way of sampling dimension spaces that have a high element of uncertainty. It can also be used for a number of functions that include using Bayesian and Likelihood distributions to estimate parameters, conduct statistical inferences and can accommodate huge observations of data. The failure analysis approach that was employed in this study utilizes a method for estimating the sensitivity of the parameters and can calculate the values of the parameters.

4.4 Descriptive Failure Analysis

As noted from figure 4.1, showing the 540 runs that were done of the Latin hypercube, dense and uniform features were observed and these were noticed also to be common among the other parameters. Figure 4.1 was presented in one-dimensional form because it was difficult to present them in three dimensional views. The most important observation that could be made is that a high level of failure is high at low points of *background_vdcl* and high points *vconst_2* and v*const_corr* parameters. On the other hand, *convect_corr* has being associated with insignificant or weaker failures. As noted by Smith et al. (2010), momentum equations can be combined with anisotropic

horizontal viscosity parameterization to come up with *vconst_2* and *vconst_corr*, these have also been observed with figure 4.1. However, the Reynold's number has been a major constraints to the parameters as their lower bounds have been subject to stability and process challenges. Thus according to Jochum et al. (2008), there is a need to incorporate the Munk boundary layer constraint which relates diffusion and advection. On the other hand, similar examinations made by Griffics (2004), that the Courant–Friedrichs–Lewy (CFL) which is viscous and relies on grid resolution and integration step time, has been constraining the upper bounds to diffusion stability. Hence, the main reason for the failures can thus be noted to be limits caused by the CFL and are triggered by the parameters' high values. In this study, the integration time was set at 1 hour. Meanwhile, the KPP vertical mixing parameterization was set using the background diffusivity for diapycnal mixing (that is, the *bckgrnd_vdc1*), (Griffics, 2004).

Numerical instability in this case is caused by a surge in the solution's numerical noise and this is as a result of having declining not only *bckgrnd_vdc1* values but also of other similar parameters. When it comes to the KPP vertical mixing scheme, viscosity and diffusivity will only increase when *convect_corr* increases in value. Smith and McWilliams (2003), established that this will cause the vertical density profile to destabilize. On the other hand, it can also be noted that the causes of failure are tied to the relationship between simulation outcomes and parameter outcomes but Danabasoglu et al., (2012), considers that it is difficult in most cases to determine the causes of failures. Observations noted from figure 4.1 do however point that parameter values and failed simulations are highly correlated. For example, it can be noted that at low points of *bckgrnd_vdc1* and high point values of *vconst_corr* there is a strong presence of failures and these are found in different sections of POP2. *Vmix_kpp* is linked with *bckgrnd_vdc1* while the *hmix_aniso* part is related to *vconst_corr*. Thus, POP2 users and developers will to some extent face difficulties in determining and simulating failures of such parameters (Smith & McWilliams, 2003).

Serious difficulties can be noted when at the low dimensional projections of figure 4.1 where failures and successes overlap. There is however mixed or various reactions of the failures. For instance, other simulations succeeded close to the parameter space while others failed and vice versa. High levels of failures and successes are concentrated between *vconst_2* and *vconst_corr* on the top right part of the scatterplot and at the lower left part of the scatterplot there are traces of isolated failures. This implies that overlaps in the statistical model are more likely to

misspecification problems and parameter values are in this case taken as the major determinant of failures. Moreover, misspecifications in this case can be in two forms. Firstly, there are what are known as false positives and this occurs when models report failures and yet in actual fact there are successes (Prati et al., 2004). Type II errors are known as false negatives and they occur when it considers to be success yet in actual fact there is going to be failures. In some instances, class overlaps will occur when there is a population mismatch between two or more populations (data imbalances) and such imbalances will be highly visible in the POP2 outcomes (Prati et al., 2004). As a result, robust statistical approaches that are more detailed and can provide more insights about the failures are usually required. Thus this study adopted diagnostics and algorithms that can detect signals, allow machine learning and recognize patterns. These methods are of significant importance as they make it feasible to determine simulation failures before they occur and can also allow their causes can to be quantified. This can in turn be used to make improvements to POP2 thereby causing to cater for huge changes in the parameters (Kotsiantis, 2007).

4.5 Probabilistic Failure Classification

POP2 simulations can either fail or succeed for any given combination of model parameters. Such outcomes can be presented by what is known as a two-class categorical variable. With such a variable, success is denoted by class K_S and failure by class K_F. Also with this classification, there is only one failure class but recognition has been made that simulation failures are bound to occur for various reasons. Chang and Lin (2011), outlined that failure can occur as a result of numerical instabilities, poor iterative convergences etc. the two-class categorical approach can thus be incorporated to deal with various types of failures through class classification.

The main aim behind probability class classification is to ascertain the chances that the POP2 simulation is bound to fail given vectors A = (a_1, a_2, ...a_{18}). This can be expressed using a conditional probability $\rho(K_F/ a_1)$. Applying Bayes principle, the conditional probability can be stated as follows;

$$\rho(K_F/ a_1). = \frac{p\,(a/K_f)\,p(K_f)}{p\,(a/K_f)p\,(K_f)+p\,(a/K_s)p(K_s)} \qquad (4.2)$$

Class priors and class conditional densities are respectively denoted by $\rho(C_F)$ and $\rho(a/K_F)$. A likelihood ratio can be obtained by incorporating a natural logarithm λ which can be ascertained using the formula;

$$\lambda = \left[\frac{p(a/K_f)}{p(a/K_s)} \frac{p(K_f)}{p(Ks)} \right]$$ (4.3)

By taking a logistic sigmoid function, Eq. (4.2) can be expressed as follows;

$$\rho(K_F/a) = \frac{1}{1+\exp(-\lambda)}$$ (4.4)

Failure Probability
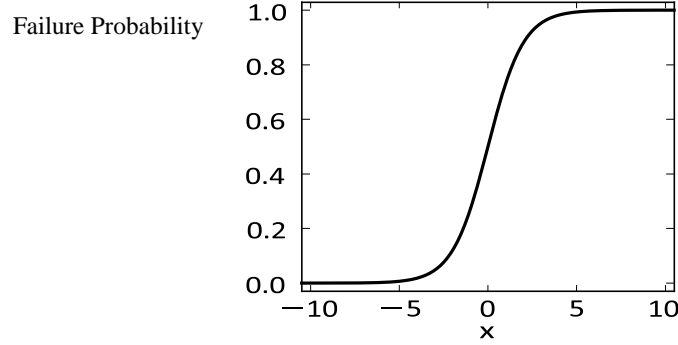
Figure 4.2: Logistic sigmoid function

The sigmoid function ranges from 0-1 while λ has values that are within $-\infty$ to ∞. However, the sigmoid function makes it possible to a probability that can be used to determine the probability of success or failure through transformation into an input vector. The logistic sigmoid function of Eq. (4.4) is shown in figure 4.2.

It must be noted that these given statistical approaches can be used in different and broader circumstances (Kotsiantis, 2007). However, a geo-scientific model that is associated with significant variations is more subject to potential failure by subjecting the output to discretization. Meanwhile, both chances of success and failure can occur at various areas of the bins or areas of the threshold. For example, when simulation of a climate model is subjected to a 5K change in average global temperatures there are high chances of an excessive case. When such occurs success or failure can take place when model instances are below or above the threshold (Chang and Lin, 2011). The chances of a model failing are provided by Eq. (4.4) and this can be established when simulated temperatures fall above the 5K par. Figure 4.3 provides a description of the kernel transformations in SVMs.
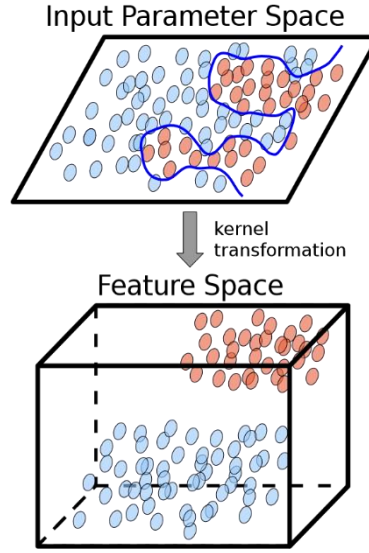
Figure 4.3: Kernel transformations in SVMs

4.6 Supervised Learning, Training and Testing

The 3 UQ studies that are shown in table 4.2 were done consequently one after the other and the classifiers was trained so that it will be easy to understand simulation failures. The main aim was to allow it to predict simulation failure before starting simulation of study 3. The training constituted of 328 successes and 32 failures all from the combined 360 simulations of studies 1 and 2. The study made use of bagging (Dietterich, 2000) also known as the bootstrap aggregation approach and this is because the number of classifiers (18) was higher that the number of failures recorded (32). Secondly, it was used because it enables one to express the response of the classifiers in numerical terms and this is important because it makes it possible to boost the performance of the classifiers (Fawcett, 2006). The initial process involved a resampling of the data which resulted in duplication of the samples and was done 100 times. As a result, various 100 versions of training data were utilized to come up with a team of SVM classifiers. In order to make failure predictions, equal weights were assigned to the votes made by the SVM team for all the classifiers. The standard deviation and mean were also computed out of this process

$$U_C = \frac{1}{Nb}\sum_{i=1}^{Nb} Pi(Cf\backslash x) \qquad (4.5).$$

$$\alpha^2_c = \frac{1}{Nb}\sum_{i=1}^{Nb} Pi(Cf\backslash x) - \pi^2] \qquad (4.6).$$

The study used LIBSVM in the training process because it allows v-support and c-support to be computed. This was also done in conjunction with hyperbolic tangent, Gaussian, polynomial and linear tangent. Other kernels were tested but a $K(x_i, x) = \exp(-y\|x_i - x\|^2)$ – Gaussian kernel of c-classification was used because of experience and familiarity. Arlose and Celisse (2010), proposed a cross validation method that can be used to determine SVM values of C (misclassification penalty), y (kernel width). Classifiers were tested using 20% of the data while the remaining 80% of the data for all the repeated training was randomly selected to develop individual classifiers. As a result, one huge cross validation test was obtained and it comprised of (*100 repeated sample x 360 simulations x 0.2 test fraction*). This was used to estimate AUC score and the ROC curve as shown in figure 4.4. The ROC was estimated using maximized values. That is, AUC = 0.94, C = 3 and y = 0.1.
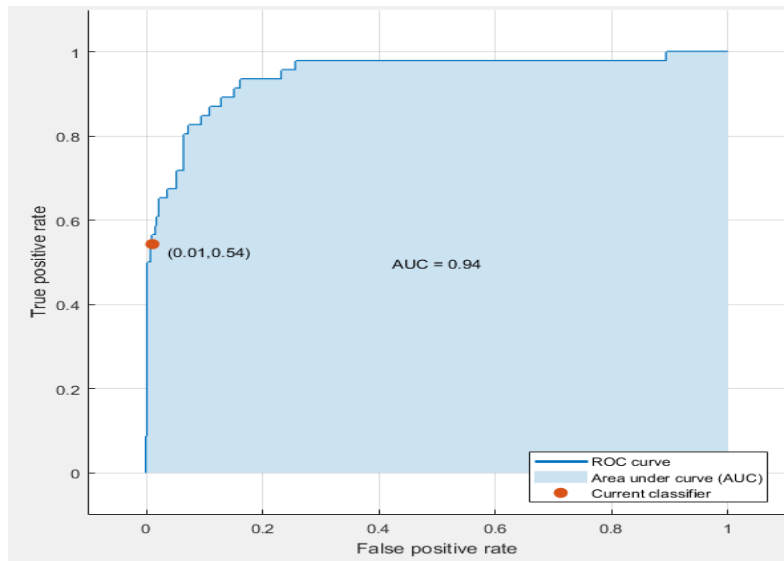
Figure 4.4: Training classifiers' SVM ROC

From figure 4.4, it can be noted that the area under the curve is high above 0.8 and thus conclusions can be made that the used training can effectively predict study 3' simulation crashes.

The entire analysis was presented through the use of Gaussian kernels but the classifiers were retrained using similar cross validation and training data, and applying hyperbolic, cubic and linear tangent kernels so as to determine the sensitivity in relation to the nature of SVM kernel. Observations can be made that all the kernels had cross validation scores that were above 0.92 but

the performance of the Gaussian kernels was way higher. Both non-linear and linear kernels showed signs of good performance and C_S and C_F were established to be linearly separable.

4.7 Neuro-Fuzzy Model Results

The four cases of the fuzzy neural algorithm that were conducted, success rates were observed to be averaging high above 92%. The highest accuracy rate can be observed to be associated with activity 4 with a success rate of 95.55% and is composed of 16 neurons.

Table 4.3: Neuro Fuzzy model results

No.	Neurons	epoch	Learn-rate	SSE_{Train}	$RMSE_{Train}$	$RMSE_{Evaluation}$	SSE_{Test}	$RMSE_{Test}$	Accuracy
1	8	500	0.003	388.19	0.3791	0.3790	76.920	0.377	92.04%
2	16	500	0.003	299.91	0.3332	0.3333	59.590	0.332	94.63%
3	8	500	0.004	388.37	0.3793	0.3781	76.396	0.376	92.22%
4	16	500	0.004	281.62	0.3229	0.3228	55.781	0.321	95.55%

Model 4 which had 16 neurons was established to be the best model in terms of accuracy and this follows a recorded accuracy rate of 95.55% while model 3 had the lowest accuracy rate of 92.22%. Root mean square errors (RMSE) indicate that the difference between the actual values and the predicted values of the train and that of the evaluation are the same for cases 1 and 3 and between 2 and 4.

Though RMSE can be noted to be declining with the number of increase in the total simulations done, it is important to note that case 1 and 3 have higher RMSE score than case 3 and 4 and this can suggest a high performance score in case 1 and 3.
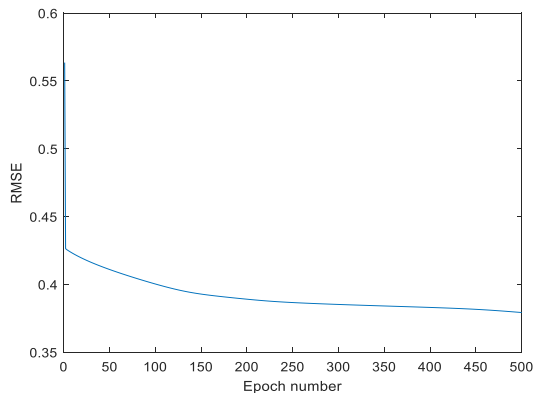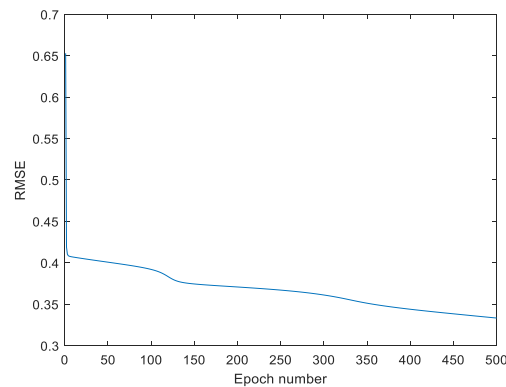
Case 1   Case 2
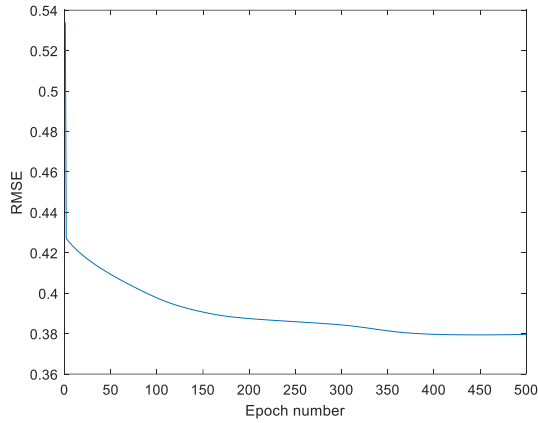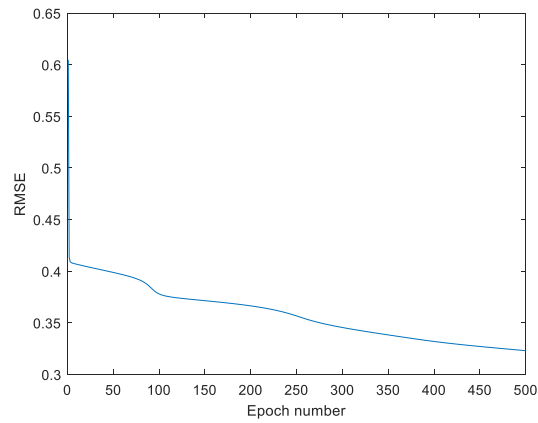
Case 3   Case 4

Figure 4.5: NFM The cases results

4.8 SVM Results

Six cases were used for the SVM algorithm with a 10-fold cross-validation and all the cases have attained an accuracy rates that are above 91%. The highest accuracy rate of 94.1% can be noted to be in line with a quadratic SVM while the lowest rate of 91.5% is recorded for Fine Gaussian SVM and Coarse Gaussian SVM.

Table 4.4: SVM results

No	Types SVM	Cross-Validation	Accuracy
1	Linear SVM	10-Fold	93.1%
2	Quadratic SVM	10-Fold	94.4%
3	Cubic SVM	10-Fold	94.1%
4	Fine Gaussian SVM	10-Fold	91.5%
5	Medium Gaussian SVM	10-Fold	91.7%
6	Coarse Gaussian SVM	10-Fold	91.5%

The best one is Quadratic SVM, Accuracy with 10-Fold Cross-Validation is 94.4%. The prediction speed is ~3100 obs/sec and training time 5.5387 sec.

4.8.1 Predicting Simulation Failures

In order to predict simulation failure, study 1 and 2 SVM classifiers training was utilized prior to conducting the 180 simulations. The predictions were emailed to the respondents and they are

shown in table 4.5. Equations 7 and 8 were utilized to determine the predictions. The following decision criteria was used to assign the simulations to C_f;

$$D \equiv threshold \ \leq decision \ variable \tag{4.9}$$

A similar threshold was utilized to select the 2 criteria. The criterion average was utilized for the initial criteria denoted by equation 10.

$$D_{avg} \equiv 0.5 \ \leq \mu_c \tag{4.10}$$

$$D_{sum} \equiv \ 0.5 \ \leq \sigma_c + \ \mu_c \tag{4.11}$$

The second criterion utilizes standard deviation and sum of the averages of the committee as shown by equation (11). The use of equation (11) is because of its ability to establish the variability of committee members and using a given number of simulations that were assigned as C_f irrespective of the fact that they had a mean below 0.5.

The results of the actual and predicted outcomes are exhibited in table 4.5 and figures 4.6. From table 4.2, it can be noted that 166 simulations were recorded as successes and 14 failures. The D_{sum} and D_{avg} classifiers showed signs of good performance.

Based on the established confusion matrix shown in figure 4.6, it can be noted that 174 correct predictions were made with an accuracy of 96.7% (TN + TP). The incorrect predictions were spread between the 2 criteria. Incorrect predictions (FN + FP) were established to be 6 but an equal number of FP and FN was found to be associated with D_{sum} while D_{avg} had a lower number of FPs than FNs. As a result, D_{sum} and D_{avg} have different patterns in the ROC. For instance, (3/166, 11/4) coordinates are associated with D_{sum} while (1/166, 9/14) are linked with D_{avg}.

TP	FP
$D_{avg} = 9$	$D_{avg} = 1$
$D_{sum} = 11$	$D_{sum} = 3$
$D_{snr} = 12$	$D_{snr} = 2$
FN	TN
$D_{avg} = 5$	$D_{avg} = 165$
$D_{sum} = 3$	$D_{sum} = 163$
$D_{snr} = 2$	$D_{snr} = 164$

Figure 4.6: Confusion matrix for predictions of the 180 simulations

Table 4.5: Study 3 simulated outcomes and predictions

Run	σ_c	μ_c	Actual	Predicted*		
				D_{snr}	D_{sum}	D_{avg}
002	0.13	0.47	Success	Success	Failure	Success
006	0.14	0.54	Failure	Failure	Failure	Failure
015	0.10	0.37	Success	Success	Success	Success
017	0.12	0.42	Failure	Success	Failure	Success
027	0.09	0.25	Failure	Success	Success	Success
044	0.02	0.04	Failure	Success	Success	Success
060	0.10	0.80	Failure	Failure	Failure	Failure
073	0.15	0.52	Failure	Failure	Failure	Failure
088	0.11	0.63	Failure	Failure	Failure	Failure
095	0.15	0.47	Success	Success	Failure	Success
097	0.09	0.83	Failure	Failure	Failure	Failure
120	0.13	0.49	Failure	Success	Failure	Success
141	0.09	0.88	Success	Failure	Failure	Failure
148	0.12	0.76	Failure	Failure	Failure	Failure
155	0.08	0.31	Failure	Success	Success	Success
166	0.11	0.64	Failure	Failure	Failure	Failure
173	0.12	0.75	Failure	Failure	Failure	Failure
177	0.14	0.67	Failure	Failure	Failure	Failure

Employing a perfect classifier, $[(TPR - 1)^2 + FPR^2]^{0.5}$, conclusions can be made that the performance of D_{avg} with an interval of 0.357 is lower than that of D_{sum} which had an interval of 0.215.
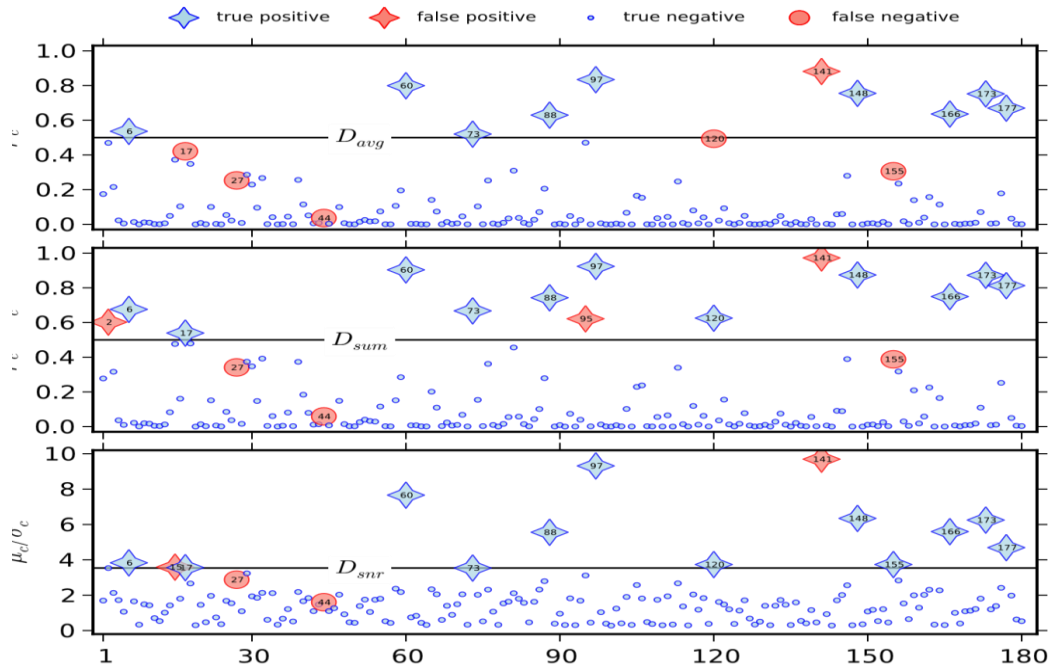
Figure 4.7: Actual and predicted outcomes confusion of the 180 simulations in Study 3

In order to determine the differences in performance, middle and top panel shown in Figure 4.6 through the use of $\sigma c + \mu c$ and μc as shown by the horizontal lines (decision criteria). Runs bellow the lines denote success while those above on the lines signify failure. Incorrect predictions are also depicted by the red dots while correct predictions are in blue. Figure 4.7 shows that D_{avg} classified runs like 17 and 120 due to failure and had lower μc values that are less than 0.5. These runs were however classified to the right class by D_{sum} but the problem was that diagnosis problems were noted with runs 2 and 95 as shown. Thus, differences in performance can be attributed to the threshold value and if 0.4 was assigned as the threshold value instead of 0.5 similar results with D_{sum} will be attained.

Using ideas given by Edwards et al. (2001), comparisons in predictive performance was made for the second study. Comparisons were not however made with the first study because they made use of the same data (evaluation and train). The approach by Edwards et al. (2001), only provides FN and TN values used for simulation predicted to fail. FN(TN + FN) was used to predict success and by comparison, this study only misclassified 2 and 3% of the successful predictions utilizing D_{sum} and D_{avg} respectively.

4.8.2 Retrospective Analysis of Simulation Failures

Decision variables σc and μc and a signal-to-noise ratio to determine the performance of the criterion using an SVM panel. However, simulation failures were not predicted before the decision due to limited information of the threshold. However, similar values of σ_c and μ_c were used in the same manner they were used to the other criteria and tests were conducted to determine if these values have a threshold that would reduce failure outcomes as well as the maximize the accuracy. As result, the following criterion whose performance is shown in table 4.3, was established;

$$D_{snr} \equiv \frac{\mu_c}{\sigma_c} \geq 3.53 \tag{4.12}$$

The performance of D_{sum} and D_{avg} is lower than that of D_{snr} and when incorporated into this study, this will give an accuracy of 97.8% with 4 false predictions which are equally distributed between 2 FPs (runs 15 and 141) and 2 FNs (runs 27 and 44) and 174 correct predictions. An interval of 0.143 is observed to be associated with D_{snr} and lies on (2/166, 12/14) from the perfect classifier on the ROC. Differences in performance are illustrated in figure 4.5. Irrespective of the idea that successes and failures are better separated by the signal-to-noise ratio but huge misclassification can be noted with runs 44 and 141. Neither D_{sum} nor D_{avg} had more simulations lying closers to them as compared to D_{snr}. Implications can therefore point to the idea that D_{snr} has a high rate of variability to changes in the threshold values. In order to determine the TPRs and FPRs of study 3, different thresholds values were utilized. The criteria's fixed locations and ROC are exhibited in figure 5.5 and it is noted that there is an overlapping between $\mu_c + \sigma_c$ and μ_c. this justifies that these variables tend to perform similarly irrespective of the threshold values used. $\mu_c + \sigma_c$ can be noted to be performing much better than μ_c as evidenced by the AUC scores. An AUC score of 0.966 was obtained for the μ_c/σ_c ROC curve. This is because it has a lower potential of identifying a huge number of TPs and is highly effective when separating classes. Overall conclusions do point out that all the 3 decision variables do perform quite well.

4.9 Sensitivity Analysis of Simulation Failures

Having successfully illustrated the how successful the study predictions are, the classifier committee was utilized to identify, ascertain the quantity and order of the model variables that were necessitating failures. This is important because such information will be utilized to improve the robustness of the model variables to perturbations by dealing with modules that are highly

sensitive. Thus, an 18 POP2 was represented by a 104 Latin hypercube samples which were determined using the average probability of failure of the committee SVM of all the points. The study then followed propositions made by Helton et al. (2006), to undertake a global sensitivity analysis. From the 540 simulations, a new panel of 100 SVM classifiers was used for the retraining exercise using methods outline in the methodology part of this study. The sensitivity analysis exercise was done using (μ_c/σ_c) and μ_c, a panel response.

4.10 Polynomial Chaos Expansion of the Failure Probability

Sobol indices developed by (Sobol, 2001), to determine the sensitivity of the variables. Such indices help to separate the variations of μ_c as contributions made by high order combination coefficients and other variables. This was achieved by using polynomial chaos expansions which is essential because it gives parameters with proportional squares which is considered to be highly convenient (Salteli et al., 2006). A second-order polynomial chaos expansion with the following expression was used;

$$\text{Log } \mu_c = a_0 + \sum_{i=1}^{Np}[b_i P_i(\xi i) + C_i P_2(\xi i)] + \sum_{i=1}^{Np-1} \sum_{j=i=1}^{Np} d_{ij} P_i(\xi i) P_i(\xi i) \tag{4.13}$$

The required coefficients are denoted by **a_0, b_i, c_i** and **d_{ij},** n-th order orthogonal polynomial of ξi is denoted by **$P_n\xi i$** and the random variability of **i** is captured by ξi captures random variability. This expression was estimated based on ideas given by Xiu and Karnidakis (2002), which established that **$P_n\xi i$** will represents shifted Legendre polynomials when standard uniform random variables are denoted by ξ_i and thus resulting in the following expression;

$$\int_0^1 P_m(\xi_i) P_n(\xi_i) d\xi_i = \frac{1}{2n+1} \delta_{mn}, \tag{4.14}$$

1st and 2nd order shifted Legendre polynomials are denoted by;

$$P_1(\xi i) = 6\xi i^2 - 6\xi i + 1 \tag{4.15}$$

$$P_2(\xi i) = 2\xi i - 1 \tag{4.16}$$

δ_{mn} is the Kronecker delta function.

The least squares approach was used to determine the coefficient of the eqn. (13). The results showed that the model has an R2 = 0.98 translating to changes in the dependent variable being explained by the model parameters. The variance is given by;

$$\text{var}(\log \mu_c) = \overbrace{\sum_{i=1}^{N_p} \left(\frac{b_i^2}{3} + \frac{c_i^2}{5} \right)}^{N_p} + \overbrace{\sum_{i=1}^{N_p-1} \sum_{j=i+1}^{N_p} \frac{d_{ij}^2}{9}}. \tag{4.17}$$

While the average mean value is computed as follows;

$$\text{avg}(\log \mu c) = a0, \tag{4.18}$$

Eqn. (14), is developed to establish values of the squared polynomial chaos expansion coefficients and the right hand side shows pairs of parameter and linear and quadratic parameters (individual parameters).

Table 4.6: Polynomial chaos expansion of failure probability.

Expansion	Leading terms*
ξ_i	$\log \mu_c \approx -4.347 + 4.049\,\xi_1 + 3.400\,\xi_2 + 2.267\,\xi_{13} - 1.980\,\xi_{14} - 1.393\,\xi_{16} - 1.253\,\xi_5 - 1.143\,\xi_4 - 1.007\,\xi_{17} - 0.885\,\xi_2\,\xi_1 - 0.796\,\xi_{13}\,\xi_1 - 0.739\,\xi_6 - 0.637\,\xi_{13}\,\xi_2 - 0.610\,\xi_9 + 0.578\;\xi_{14}\;\xi_2 + 0.480\;\xi_{16}\;\xi_2 - 0.471\;\xi_{15} - 0.414\;\xi_1^2 + 0.382\;\xi_5\;\xi_1 + 0.372\;\xi_{14}\;\xi_1 + 0.351\,\xi_{17}\,\xi_2 + 0.320\,\xi_2\,\xi_5 + 0.320\,\xi_8^2 + \ldots$
$P_n(\xi_i)$	$\log \mu_c \approx -2.609 + 1.628\,P_1(\xi_1) + 1.546\,P_1(\xi_2) + 1.061\,P_1(\xi_{13}) - 0.895\,P_1(\xi_{14}) - 0.475\,P_1(\xi_5) - 0.455\,P_1(\xi_{16}) - 0.338\,P_1(\xi_4) - 0.311\,P_1(\xi_{17}) - 0.245\,P_1(\xi_9) - 0.221\,P_1(\xi_1)\,P_1(\xi_2) - 0.199\,P_1(\xi_1)\,P_1(\xi_{13}) + 0.196\,P_1(\xi_{12}) + 0.174\,P_1(\xi_{10}) + 0.164\,P_1(\xi_{11}) - 0.159\,P_1(\xi_2)\,P_1(\xi_{13}) + 0.145\,P_1(\xi_2)\,P_1(\xi_{14}) + 0.133\,P_1(\xi_{18}) + 0.120\,P_1(\xi_2)\,P_1(\xi_{16}) + 0.096\,P_1(\xi_1)\,P_1(\xi_5) + 0.093\,P_1(\xi_1)\,P_1(\xi_{14}) + 0.088\,P_1(\xi_2)\,P_1(\xi_{17}) - 0.082\,P_1(\xi_6) + \ldots$

*

4.11 Sensitivity Network of the Failure Probability

Network graphs with edges and nodes were utilized as a strategy that aids in analyzing complex variance linkages. Fractional composition of parameter i, is proportionally related to the magnitude of node i.

$$\text{Node i} =^i \propto \frac{b_i^2/3 + c_i^2/5}{\text{var}(\log \mu)} \tag{4.19}$$

Part of the contribution of the joint variation of the coefficients j and I is proportional node j, connecting node i and the thickness of the edge ij.

$$\text{Edge}_{ij} = {}^{ij} \propto \frac{ij/9}{\text{var}(\log \mu\ )} \tag{4.20}$$

It must be noted that this method does consist of 3rd order terms and among others edge$_{ijk}$ (higher effects) but will not be used in the estimation process. Long nodes are a representation of essential parameters of the developed network graph and have a tendency to produce significant linkages with other nodes.
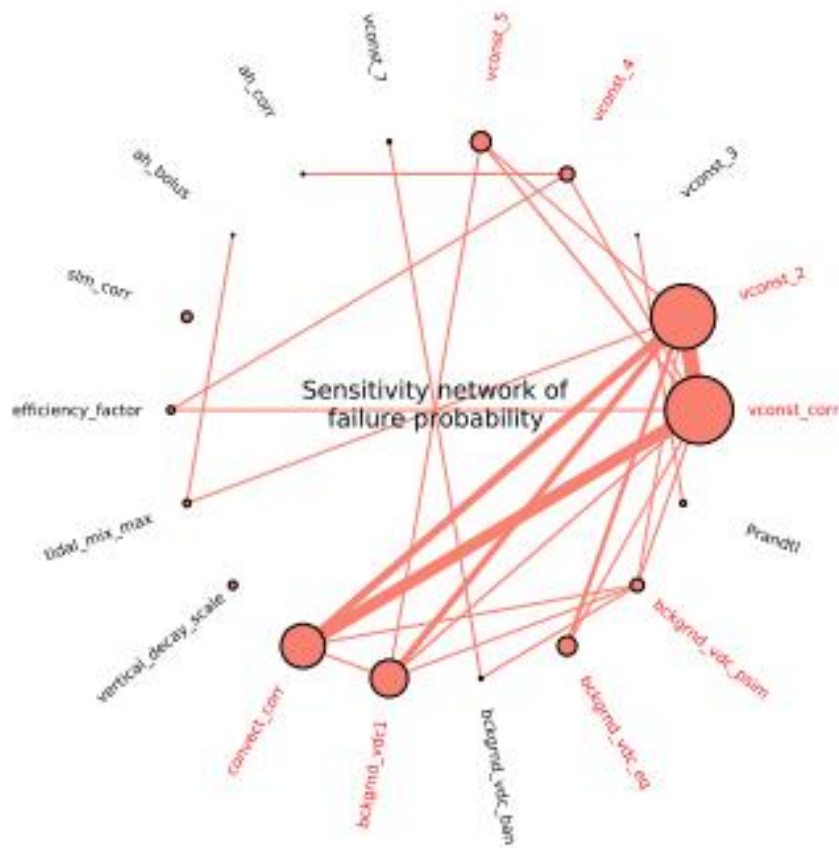
Figure 4.8: Network graph showing sensitivity of the probability of simulation failure

Figure 4.8, is a pictorial description of the variance decomposition of Logμ_c. When using node connectivity and size, the results exhibit that 8 of the 18 coefficients are necessitating major simulation failure as denoted by coefficients in red colour. These were responsible for 95% changes that were observed with logμ_c as illustrated by eqn. (18). The four parameters whose

results were remarkable are *bckgrnd_vdc1, convect_corr, vcost_2* and *vcost_corr*. They can also be concluded to be having highly connected and huge nodes and they constitute 88% of the variations observed with $\text{Log}\mu_c$. A strong connection provides evidence that the probability of simulation failure is determined by the co-movements that tend to heighten failures. Thus, eqn. (18), provides an indication of the impact of the coefficients on simulation failures by ranking them. This offers ways that can be used to make improvements to the model. In addition, co-movements between the simulation failures and the parameters values are shown by the scatterplot by they are not adequate enough to distinguish overlapping C_S and C_f classes. Moreover, it exhibits that at least more than four coefficients are needed to offer explanations and distinguish simulation successes from failures.

4.12 Learner Regression Analysis

Vconst_3 and vconst_4 can be said to have been accurately predicted by the model and this follows the idea that the residuals are almost closely and symmetrically distributed across the lines. Thus the model can be said to be poorly capable of predicting Vconst_1 and vconst_2 responses.
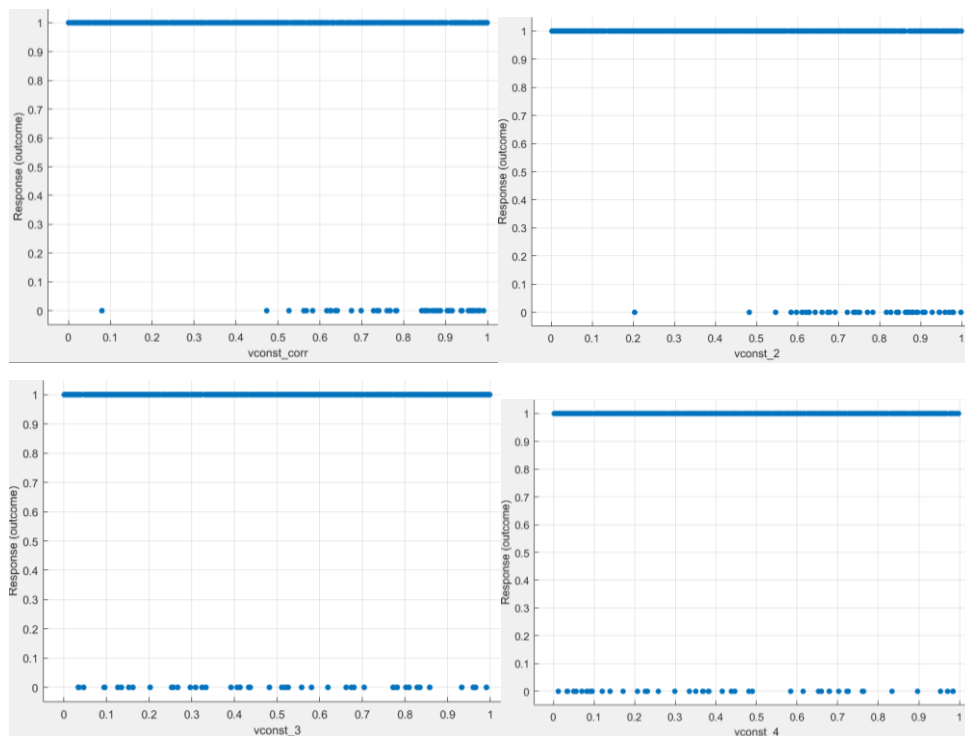
Figure 4.9: Simulation outcomes

4.13 Model Performance

After training, model performance of the estimated Leaner regression model was determined using prevailing results of the model scores which shows which model has the best overall score. Such a score is termed the root mean square error (RMSE) on the validation set alternatively, it can be said to be useful in estimating the performance of the trained model on new data. A 10-fold cross validation was used for all the SVM models and the results show that the Fine Gaussian SVM offers the best simulation performance. This is because it has a lower RMSE of 0.23 compared to other SVM types such as Cubic SVM which had RMSE of 0.23. The training time took 17.216 sec and the results through R-Squared showed that 0.35 of the simulation failures is explained by the estimated SVM. The obtained MAE and MSE were recorded to be 0.15 and 0.05 respectively.

Table 4.7: Model performance of the SVM types

No	Types SVM	Cross-Validation	RMSE
1	Linear SVM	10-Fold	0.27
2	Quadratic SVM	10-Fold	0.24
3	Cubic SVM	10-Fold	0.23
4	Fine Gaussian SVM	10-Fold	0.29
5	Medium Gaussian SVM	10-Fold	0.23
6	Coarse Gaussian SVM	10-Fold	0.27

Response plots were used to determine which model offers the best performance in terms of the predictability power. The decision criteria is to accept that the model is a good model and can forecast or predict the actual actual when the resultant distance or margin between the actual and predicted values is small.
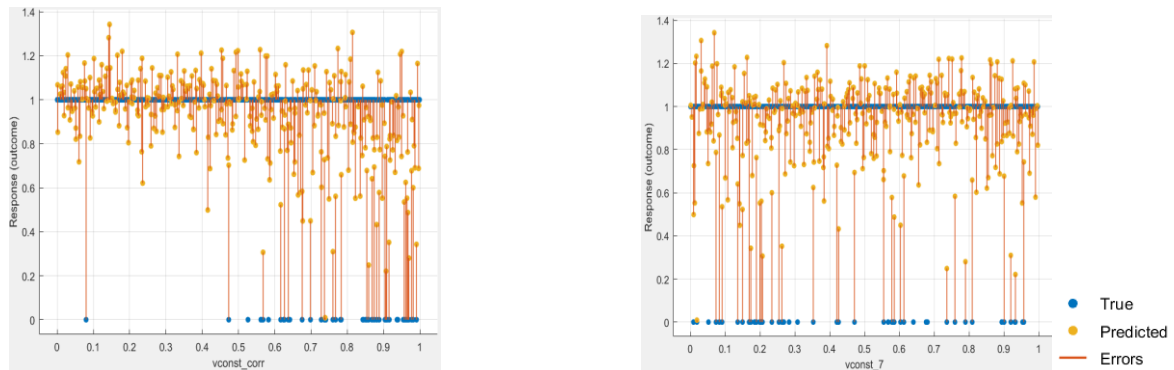
Figure 4.10: Response plots

The response outcome is high for vconst predictions and can be considered to be having a high predictability power at lower values but falls as more vconst_corr values are added in to the analysis. Meanwhile, the opposite can be said about vconst_7 which low predictive capacity at low vconst_7 values but later increases as more because are units are included in the analysis. However, the estimated model can be said to be good at predicting vconst_7 response values because its residuals (errors) are almost symmetrically distributed across the line.

CHAPTER 5.
CONCLUSIONS AND SUGGESTIONS

The main emphasis of the study was to determine if there are any crashes or failure that are associated with the use of simulation models as well as conditions that can cause climate models to fail by determining the chances that POP2 simulation will fail. Thus Support Vector Machines (SVM) and fuzzy neural were used to determine chances of failure of the models.

During the process of carrying out Latin hypercube ensemble simulations involving viscosity and ocean mixing parameters drawn from POP2 elements of the CCSM4, code crashes were observed to be relatively visible. The occurrence of the crashes was established to be due to several numerical reasons which were caused by changes in the combination of the parameter values used in the simulation process.

The simulation crashes were based on the idea that they may either succeed or fail (binary problem) and failure probabilities were quantified using machine learning classification. The quantification process was based on the 18 model parameters and of the 360 simulations that were made, 32 simulations were recorded as failures while the rest was considered to be successful. The validation process was conducted using 180 independent simulations.

The established confusion matrix it was noted that 176 correct predictions were made with an accuracy of 97.8% while incorrect predictions were spread between the 2 criteria. Incorrect predictions (FN + FP) were established to be 6 but an equal number of FPs and FNs was found to be associated with Dsum while Davg had a lower number of FPs than FNs.

Based on the classification system that was used, it was discovered that a prediction score above 0.94 was recorded for AUC with at least 0.94 discrimination competence. From the available four modules which had a high potency to fail, eight model parameters were retrieved and the results can be utilized to enhance the effectiveness of CCSM4 when exposed to parameter perturbations. Such is important because it can be used in different scenarios with complex models.

Finally, a comparison was made between SVM and neuro-fuzzy model results to determine which algorithm offers the best simulation results. Accuracy rates of 94.4% and 95.55% were obtained

for SVM and neuro-fuzzy model of the simulations. Thus it can finally be concluded that fuzzy-neural network performs better in modelling climate crashes as compared to SVM.

REFERENCES

Abiyev, R. (2003). Fuzzy inference system based on neural network for technological process control. Mathematical and Computational Applications, 8(2), 245-252.

Abiyev, R. H. (2003, July). Recurrent neural network based fuzzy inference system for identification and control of dynamic plants. In Proceedings of International XII Turkish Symposium on Artificial Intelligence and Neural Networks (Vol. 1, No. 1, pp. 31-39).

Abiyev, R. H. (2005). Neuro-fuzzy system for equalization channel distortion. International Journal of Computational Intelligence, 229-232.

Abiyev, R. H. (2009). Fuzzy wavelet neural network for prediction of electricity consumption. AI EDAM, 23(2), 109-118.

Abiyev, R. H. (2014). Credit rating using type-2 fuzzy neural networks. Mathematical Problems in Engineering, 2014.

Abiyev, R. H., & Abizade, S. (2016). Diagnosing Parkinson's Diseases Using Fuzzy Neural System. Computational and mathematical methods in medicine, 2016.

Abiyev, R. H., Aliev, R., Kaynak, O., Turksen, I. B., & Bonfig, K. W. (2015). Fusion of computational intelligence techniques and their practical applications. Computational intelligence and neuroscience, 2015.

Abiyev, Rahib H., Nurullah Akkaya, Ersin Aytac, Irfan Günsel, and Ahmet Çağman. "Brain-Computer Interface for Control of Wheelchair Using Fuzzy Neural Networks." BioMed research international 2016 (2016).

Artale, V., Calmanti, S., Carillo, A., Dell'Aquila, A., Herrmann, M., Pisacane, G., ... & Bi, X. (2010). An atmosphere–ocean regional climate model for the Mediterranean area: assessment of a present climate simulation. Climate Dynamics, 35(5), 721-740.

Beaumont, L. J., Hughes, L., & Pitman, A. J. (2008). Why is the choice of future climate scenarios for species distribution modelling important?. Ecology letters, 11(11), 1135-1146.

Berenji, H. R. and Khedkar, P. (1992). Learning and Tuning Fuzzy Logic Controllers Through Reinforcements, IEEE Trans. Neural Networks, 3, pp. 724-740.

Berenji, H.R. (1992). A Reinforcement Learning- Based Architecture for Fuzzy Logic Con-trol. International Journal of Approximate Reasoning 6, 267--292.

Bezdek, J. C., Tsao, E. C.-K. and Pal, N. R. (1992). Fuzzy Kohonen Clustering Networks, in Proc. IEEE Int. Conf. on Fuzzy Systems 1992 (San Diego), pp. 1035-1043.

Bishop, C. (2007). Pattern Recognition and Machine Learning (Information Science and Statistics), 1st edn. 2006. corr. 2nd printing edn. Springer, New York.

Breiman, L. (2001). Random forests. Machine learning, 45(1), 5-32.

Buckley, J. J. and Hayashi, Y. (1994). Fuzzy neural networks: A survey, Fuzzy Sets and Systems 66, pp. 1-13.

Chih-Chung, C. (2011). LIBSVM: a library for support vector machines. ACM Transactions on Intelligent Systems and Technology, 2, 27-1.

Clune, T. & Rood, R. (2011). Software testing and verification in climate model development, IEEE Software, 28, 49–55.

Danabasoglu, G., Bates, S. C., Briegleb, B. P., Jayne, S. R., Jochum, M., Large, W. G., ... & Yeager, S. G. (2012). The CCSM4 ocean component. Journal of Climate, 25(5), 1361-1389.

Davies, S. M. (2003, November). Climate change: a grand software challenge. In Proceedings of the FSE/SDP workshop on Future of software engineering research (pp. 99-104). ACM.

Dietterich, T. G. (2000). Ensemble methods in machine learning. Multiple classifier systems, 1857, 1-15.

Easterbrook, S. M. & Johns, T. C. (2009). Engineering the software for understanding climate change, Comput. Sci. Eng., 11, 65–74.

Easterbrook, S. M. (2010). Climate change: a grand software challenge, in: FoSER, edited by: Roman, G.-C. and Sullivan, K. J., 99–104, ACM.

Easterbrook, S. M., Edwards, P. N., Balaji, V., & Budich, R. (2011). Guest editors' Introduction: climate change – science and software, IEEE Software, 28, 32–35.

Edwards, N. R., Cameron, D., & Rougier, J. (2011). Precalibrating an intermediate complexity climate model, Clim. Dynam., 37, 1469– 1482, doi:10.1007/s00382-010-0921-0.

Evans, J. P., & McCabe, M. F. (2010). Regional climate simulation over Australia's Murray-Darling basin: A multitemporal assessment. Journal of Geophysical Research: Atmospheres, 115(D14).

Farrell, P. E., Piggott, M. D., Gorman, G. J., Ham, D. A., Wilson, C. R., & Bond, T. M. (2011). Automated continuous verification for numerical simulation, Geosci. Model Dev., 4, 435– 449, doi:10.5194/gmd-4-435-2011.

Forrester, A., & Keane, A. (2008). Engineering design via surrogate modelling: a practical guide. John Wiley & Sons.

Fox-Kemper, B., Ferrari, R., & Hallberg, R. (2008). Parameterization of mixed layer eddies. Part I: Theory and diagnosis. Journal of Physical Oceanography, 38(6), 1145-1165.

Gent, P. R., & Mcwilliams, J. C. (1990). Isopycnal mixing in ocean circulation models. Journal of Physical Oceanography, 20(1), 150-155.

Gent, P. R., Danabasoglu, G., Donner, L. J., Holland, M. M., Hunke, E. C., Jayne, S. R., Lawrence, D. M., Neale, R. B., Rasch, P. J., Vertenstein, M., Worley, P. H., Yang, Z.-L., & Zhang, M. (2011). The Community Climate System Model Version 4, J. Climate, 24, 4973–4991.

Griffies, S. M. (2004). Fundamentals of ocean climate models (Vol. 518, No. 1). Princeton: Princeton university press.

Hagemann, S., Chen, C., Clark, D., Folwell, S., Gosling, S. N., Haddeland, I., ... & Wiltshire, A. (2013). Climate change impact on available water resources obtained using multiple global climate and hydrology models. Earth System Dynamics, 4, 129-144.

Helwan, A., Idoko, J. B., & Abiyev, R. H. (2017). Machine learning techniques for classification of breast tissue. Procedia Computer Science, 120, 402-410.

Jackson, C., Sen, M., Huerta, G., Deng, Y., & Bowman, K. (2008). Error reduction and convergence in climate prediction, J. Climate, 21, 6698–6709.

Jochum, M., Danabasoglu, G., Holland, M., Kwon, Y. O., & Large, W. G. (2008). C06017-Ocean viscosity and climate (DOI 10.1029/2007JC004515). Journal of Geophysical Research, 113(6).

Jones, P. G., & Thornton, P. K. (2013). Generating downscaled weather data from a suite of climate models for agricultural modelling applications. Agricultural Systems, 114, 1-5.

Jones, P. G., Thornton, P. K., & Heinke, J. (2009). Generating characteristic daily weather data using downscaled climate model data from the IPCC's Fourth Assessment.

Kiehl, J. T., & Shields, C. A. (2005). Climate simulation of the latest Permian: Implications for mass extinction. Geology, 33(9), 757-760.

Kotsiyiannis, I. G. (Ed.). (2007). Emerging artificial intelligence applications in computer engineering: real word AI systems with applications in eHealth, HCI, information retrieval and pervasive technologies (Vol. 160). Ios Press.

Koutsoyiannis, D., Efstratiadis, A., Mamassis, N., & Christofides, A. (2008). On the credibility of climate predictions. Hydrological Sciences Journal, 53(4), 671-684.

Lamarque, J. F., Shindell, D. T., Josse, B., Young, P. J., Cionni, I., Eyring, V., ... & Dalsoren, S. (2013). The Atmospheric Chemistry and Climate Model Intercomparison Project (ACCMIP): overview and description of models, simulations and climate diagnostics. Geoscientific Model Development, 6, 179-206.

Large, W. G., & Yeager, S. G. (2009). The global climatology of an interannually varying air–sea flux data set. Climate dynamics, 33(2-3), 341-364.

Large, W. G., McWilliams, J. C., & Doney, S. C. (1994). Oceanic vertical mixing: A review and a model with a nonlocal boundary layer parameterization. Reviews of Geophysics, 32(4), 363-403.

Leung, L. R., Qian, Y., & Bian, X. (2003). Hydroclimate of the western United States based on observations and regional climate simulation of 1981–2000. Part I: Seasonal statistics. Journal of Climate, 16(12), 1892-1911.

National Research Council Report. (2012). Assessing the Reliability of Complex Models: Mathematical and Statistical Foundations of Verification, Validation, and Uncertainty Quantification, The National Academies Press.

Prati, R. C., Batista, G. E. A. P. A., & Monard, M. C. (2004, April). Class imbalances versus class overlapping: an analysis of a learning system behavior. In MICAI (Vol. 4, pp. 312-321).

Randall, D. A., Wood, R. A., Bony, S., Colman, R., Fichefet, T., Fyfe, J., & Stouffer, R. J. (2007). Climate models and their evaluation. In Climate change 2007: The physical science basis. Contribution of Working Group I to the Fourth Assessment Report of the IPCC (FAR) (pp. 589-662). Cambridge University Press

Randall, D. A., Wood, R. A., Bony, S., Colman, R., Fichefet, T., Fyfe, J., & Stouffer, R. J. (2007). Climate models and their evaluation. In Climate change 2007: The physical science basis. Contribution of Working Group I to the Fourth Assessment Report of the IPCC (FAR) (pp. 589-662). Cambridge University Press.

Rugaber, S., Dunlap, R., & Ansari, S. (2011). Managing software complexity and variability in coupled climate models. IEEE software, 28(6), 43-48.

Stainforth, D., Aina, T., Christensen, C., Collins, M., Faull, N., Frame, D. J., Kettleborough, J. A., Knight, S., Martin, A., Murphy, J. M., Piani, C., Sexton, D., Smith, L. A., Spicer, R. A., Thorpe, A. J., & Allen, M. R.. (2005). Uncertainty in predictions of the climate response to rising levels of greenhouse gases, Nature, 433, 403–406.

Stein, M. (1987). Large sample properties of simulations using Latin hypercube sampling. Technometrics, 29(2), 143-151.

Stensrud, D. J. (2009). Parameterization schemes: keys to understanding numerical weather prediction models. Cambridge University Press.

Tannahill, J., Lucas, D. D., Domyancic, D., Brandon, S., & Klein, R. (2011, November). Poster: Data intensive uncertainty quantification: applications to climate modeling. In Proceedings of the 2011 companion on High Performance Computing Networking, Storage and Analysis Companion (pp. 17-18). ACM.

Van Vuuren, D. P., Lowe, J., Stehfest, E., Gohar, L., Hof, A. F., Hope, C., ... & Plattner, G. K. (2011). How well do integrated assessment models simulate climate change?. Climatic climate system model (CCSM) and community earth system model (CESM). Rep. LAUR-01853, 141, 1-140.

Washington, W. M. & Parkinson, C. L. (2005). An introduction to threedimensional climate modeling, University Science Books, 2nd Edn.

Watanabe, M., Suzuki, T., O'ishi, R., Komuro, Y., Watanabe, S., Emori, S., ... & Takata, K. (2010). Improved climate simulation by MIROC5: mean states, variability, and climate sensitivity. Journal of Climate, 23(23), 6312-6335.

Webster, M. D., Scott, J., Sokolov, A. P., & Stone, P. H. (2006). Estimating probability distributions from complex models with bifurcations: The case of ocean circulation collapse. MIT Joint Program on the Science and Policy of Global Change.

APPENDICES

APPENDIX A

DATASET OF CLIMATE CRASHES MODEL

Sl	Prandtl	bckgrn	bckgrn	bckgrn	bckgrnd	convect_c	vertical	tidal_mix	efficien	sim_co	ah_bolus	ah_corr	vconst_	vconst_	vconst_	vconst_	vconst_	vconst_2	ou
1	0.86989304	0.79699724	0.86931037	0.307521787	0.449620077	0.997518496	0.869090703	0.104225665	0.24567485	0.4743696	0.56794942	0.428325428	0.735936041	0.1705213	0.298838311	0.256085622	0.927824536	0.650109621	0
2	0.5122614	0.4384479	0.3657342	0.346726889	0.864151868	0.845247142	0.91434667	0.975785581	0.6768699	0.29661775	0.823014925	0.444572488	0.934850661	0.843333077	0.306957377	0.35944423	0.457728363	0.606041103	1
3	0.36585796	0.28563553	0.25064237	0.31537406	0.924775074	0.78441133	0.64335661	0.803413076	0.67935603	0.81166694	0.195928292	0.74622533	0.605570623	0.616890334	0.504992546	0.517393356	0.373238487	0.97755978	1
4	0.47598673	0.6943093	0.84592123	0.97797175	0.912819094	0.362750561	0.76658752	0.597878903	0.4774627	0.00100489	0.392132267	0.005525437	0.490827882	0.74205567	0.197532695	0.104055314	0.78340786	0.406249536	1
5	0.13228288	0.28009776	0.3766801	0.043544765	0.52226106	0.650222833	0.31234434	0.74387659	0.55754324	0.73791387	0.191926451	0.609177829	0.971206033	0.844739752	0.635636719	0.303390105	0.513199297	0.40624953	1
6	0.2940948	0.13537891	0.95412278	0.329318038	0.650677696	0.017487184	0.615967667	0.035982366	0.440094321	0.73791387	0.191926451	0.609177829	0.971206033	0.22281712	0.813407572	0.303390105	0.629025938	0.41137947	1
7	0.2181425	0.1472516	0.0125133	0.637077696	0.467358949	0.969806832	0.959217373	0.264854683	0.57981949	0.049142869	0.662635625	0.406839624	0.796645887	0.14034621	0.656415397	0.156383456	0.548838498	0.161105007	1
8	0.09273955	0.02643087	0.9265637	0.481100054	0.411672883	0.88652238	0.69477365	0.522427847	0.88676809	0.39730646	0.68377254	0.84625746	0.000445115	0.39910564	0.933182763	0.898731363	0.898731363	0.4529899	1
9	0.4872159	0.4150514	0.0622256	0.053683565	0.48839566	0.254944302	0.398823072	0.290483708	0.23652445	0.0601653	0.90993173	0.40207875	0.05636256	0.287070317	0.980120611	0.35297856	0.16675788	0.16675788	1
10	0.42002736	0.00726821	0.2208967	0.21329028	0.100291351	0.374270055	0.665368808	0.325387509	0.94560957	0.4170031	0.426141006	0.546563676	0.94759453	0.0619017	0.163485864	0.413930717	0.655620608	0.655620608	1
11	0.88487108	0.54639502	0.87084001	0.804212452	0.295425919	0.974333948	0.084268972	0.49234254	0.9711286	0.159440334	0.497766735	0.829782296	0.4578377	0.329803463	0.423497844	0.293692412	0.15900798	0.15900798	1
12	0.83358987	0.21008964	0.26988036	0.728459115	0.99967689	0.72945346	0.520566651	0.03837733	0.82841547	0.906943852	0.681179841	0.47618352	0.79100537	0.17330591	0.903222367	0.42491617	0.88192908	0.88192908	1
13	0.53198885	0.7301488	0.08139244	0.544458264	0.175169764	0.7835143	0.57781749	0.95483328	0.23098254	0.05091749	0.833960006	0.352769204	0.6765593	0.64971227	0.857328773	0.97690606	0.9610026	0.9610026	0
14	0.13568058	0.59959429	0.82044557	0.401369982	0.428806485	0.597280032	0.947346732	0.347039855	0.85378356	0.37125663	0.056095644	0.366947346	0.25445636	0.25445636	0.591358659	0.623446508	0.013556374	0.17252963	1
15	0.02844874	0.5621247	0.89335483	0.01497916	0.589646486	0.499615991	0.865611911	0.403965568	0.5100259	0.125064	0.360116875	0.78627054	0.609097664	0.609097664	0.836439982	0.96810764	0.2012425	0.3965356	1
16	0.77885351	0.3620883	0.6057303	0.922480759	0.75845499	0.29350004	0.051819288	0.25117461	0.10913853	0.59306937	0.77588936	0.231361709	0.99714749	0.433167081	0.433167081	0.909292558	0.30912551	0.05162036	1
17	0.64706519	0.9930594	0.69147824	0.226890761	0.550210882	0.247466384	0.941652686	0.586656405	0.41252405	0.75225355	0.74484045	0.938989143	0.031136722	0.98134841	0.975635677	0.702882553	0.69677366	0.81435644	1
18	0.97304947	0.37872641	0.41353844	0.239453253	0.87805461	0.820039098	0.444219065	0.644758866	0.83525191	0.65695297	0.560203906	0.729778768	0.897785418	0.9167813	0.430667284	0.794123938	0.791531254	0.55952412	1
19	0.62039197	0.55880698	0.14028424	0.578621063	0.424553435	0.231382255	0.43723928	0.083272596	0.67426918	0.14484684	0.02315243	0.179080954	0.951339673	0.13334942	0.83954677	0.868963932	0.227814194	0.453287747	1
20	0.1467012	0.25494935	0.06748964	0.41210954	0.895280358	0.89342314	0.116668505	0.97104952	0.4576951	0.09224283	0.677969692	0.41556678	0.730276729	0.66098443	0.39134176	0.408204473	0.53976397	0.3967749	1

APPENDIX B

TSK SOURCE CODE

```matlab
function [c1,o1,w1,w2]=class_nfuztsk(c1,o1,w1,w2)
% Fuzzy Neural Networks (Muti-input multi-output networks) MIN
T-norm operation
% The NEFUZM is used to create network realising Mamdany type
fuzzy system.
%   Rahib H,Abiyev, January 2001
%   Copyright by Rahib H.Abiyev


%   clustering Multioutput bsisic program, using linear function
in consequent part => TSK type
%clases start from 0. For 5 class the output classes should be
0,1,2,3,4.
% option1 - train=1,  test=2
% N1 - number of neurons of input layer
% N2 - number of neurons of rule (hidden) layer
% M - number of neurons of output layer
% a1 - learning rate
% a2 - Momentum
% maxc - output classes
% clustering  1-with clustering,  0- without clustering
menu1='T'
if(menu1=='T') load BB.txt; xt=BB(:,:); maxc=2; end    %breast
tissue
[row,col]=size(xt);
for i=1:col-1
    max1=max(xt(:,i));
    xt(:,i)=xt(:,i)/max1;
end
```

```matlab
N2=8;  tbeg=0;  tend=row;
for t=tbeg+1:tend
    Data(t-tbeg,:)=[xt(t,1:col)];
end
N1=col-1;    M=maxc;
[N1    N2    M]
pause
clc
disp('0- Initialization of parameters ')
disp('1- Learning                      ')
disp('2- Testing                       ')
disp('3- Exit                          ')
num=input('Enter number : ');
switch num
    case 0, k1=1;k2=1; k3=1; k4=1;
            [c1,o1,w1,w2]=nfuzTSKgen(N1,N2,M,k1,k2,k3,k4);
            [c1,o1,w1,w2]=class_nfuztsk(c1,o1,w1,w2)
    case 1,  epoch =500;    option1=1; clustering=0; a1=0.030;
a2=0;
[c1,o1,w1,w2]=nfuzTSKtrain_crosv(menu1,option1,N1,N2,M,a1,a2,Dat
a,epoch,maxc,clustering,c1,o1,w1,w2);
            [c1,o1,w1,w2]=class_nfuztsk(c1,o1,w1,w2)
    case 2, option1=2;epoch =1; clustering=0; a1=0.0; a2=0;
[c1,o1,w1,w2]=nfuzTSKtrain_crosv(menu1,option1,N1,N2,M,a1,a2,Dat
a,epoch,maxc,clustering,c1,o1,w1,w2);
            [c1,o1,w1,w2]=class_nfuztsk(c1,o1,w1,w2);
    case 3, quit cancel;
end
end
```